

Supporting Information - Exploring vibronic coupling in the benzene radical cation and anion with different levels of the GW approximation

S1. NON-EMPIRICAL TUNING OF THE RANGE-SEPARATION PARAMETER IN TCAM-B3LYP

A function (J^2) that measures the difference between the energy eigenvalues for the HOMO and the IP of the benzene is given by

$$J^2 = [\varepsilon_{HOMO}(N) + IP(N)]^2 + [\varepsilon_{HOMO}(N+1) + IP(N+1)]^2 \quad (1)$$

where

$$IP(N) = E(N-1) - E(N), \quad (2)$$

where ε_{HOMO} is the energy of the HOMO, N is the number of electrons in the molecule, and the IP is calculated as the Δ SCF value between the N and $N-1$ electron system. The goal of IP-tuning is then to minimise the value of J^2 for a given molecule and functional by varying the parameters in the exchange-correlation functional.

For example, the amount of exact exchange in a range-separated functional can be split into separate long and short range components using the error function (erf).

$$\frac{1}{r_{12}} = \frac{1 - [\alpha + \beta \text{erf}(\gamma r_{12})]}{r_{12}} + \frac{\alpha + \beta \text{erf}(\gamma r_{12})}{r_{12}} \quad (3)$$

r_{12} is the inter-electronic distance, α is the amount of exact exchange in the short range region, which is increased to $\alpha + \beta$ in the long range region. γ is used to classify the short and long range regions. Hence, α , β , and γ are examples of functional parameters that can be modified to minimise J^2 . Although it is possible to carry out a multi-dimensional simultaneous tuning of these three parameters, it is sufficient in practice to ‘tune’ a single parameter, γ .¹

As the interelectronic repulsion tends asymptotically towards r_{12}^{-1} in the long range region, another condition to ensure the reliability of IP-tuned range-separated functionals is to require $\alpha + \beta = 1$.² Since the standard CAM-B3LYP functional³ ($\alpha = 0.19$, $\beta = 0.46$) does not fulfil this condition, we carried out the IP-tuning procedure on the tuned CAM-B3LYP functional⁴ ($\alpha = 0.0799$, $\beta = 0.9201$) by Okuno *et al.* instead.

J^2 was calculated as γ was varied from 0.20 to 0.40 Bohr⁻¹ by carrying out single point tCAM-B3LYP and unrestricted tCAM-B3LYP calculations of the neutral, anionic and cationic forms of benzene to obtain the SCF and HOMO energies of the respective systems. A polynomial fit was then used to obtain the value of γ at which J^2 was minimised, which was found to be 0.2770 Bohr⁻¹. The above calculations were carried out with Gaussian16 and the B3LYP/def2-TZVPP optimised geometry of neutral benzene. The source code of molgw v2.D and the libxc v.4.3.4.⁵ library was also modified slightly to define the IP-tCAM-B3LYP functional.

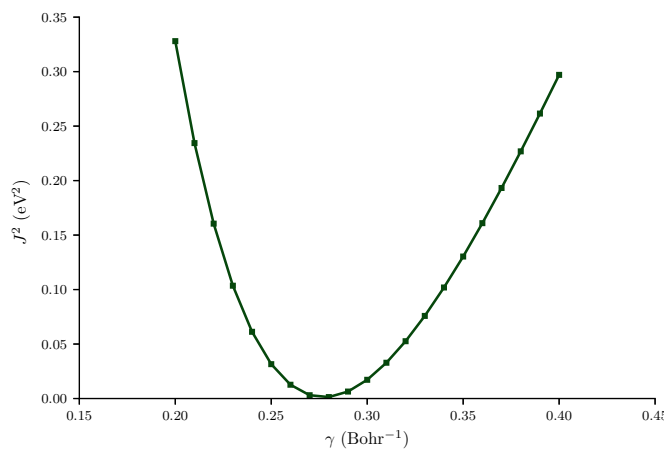


FIG. S1. Plot of the error function J^2 against γ for the tCAM-B3LYP functional in neutral benzene. The def2-TZVPP basis set was used.

S2. IP AND EA OF NEUTRAL BENZENE WITHIN DFT AND *GW*

TABLE S1. IP and EA of benzene within DFT and *GW*, calculated using the def2-TZVPP and def2-QZVPP basis sets. The qs*GW* method is not listed under any exchange-correlation functional because it is completely independent of the DFT starting point. All values are in eV.

		IP		EA	
		def2-TZVPP	def2-QZVPP	def2-TZVPP	def2-QZVPP
BLYP	DFT	6.12	6.14	0.98	1.02
	G_0W_0	8.85	8.99	-1.39	-1.14
	ev GW_0	9.06	9.24	-1.58	-1.30
	ev GW	9.28	9.45	-1.84	-1.56
B3LYP	DFT	7.06	7.08	0.40	0.45
	G_0W_0	9.05	9.19	-1.55	-1.30
	ev GW_0	9.13	9.31	-1.68	-1.40
	ev GW	9.26	9.44	1.85	-1.57
CAM-B3LYP	DFT	8.50	8.52	-0.88	-0.82
	G_0W_0	9.23	9.39	-1.73	-1.48
	ev GW_0	9.23	9.41	-1.77	-1.51
	ev GW	9.28	9.45	1.83	-1.57
tCAM-B3LYP	DFT	8.46	8.48	-0.92	-0.86
	G_0W_0	9.23	9.39	-1.66	-1.41
	ev GW_0	9.25	9.43	-1.71	-1.44
	ev GW	9.30	9.47	-1.79	-1.52
IP-tCAM-B3LYP	DFT	9.41	9.43	-1.56	-1.49
	G_0W_0	9.32	9.48	-1.76	-1.51
	ev GW_0	9.30	9.47	-1.78	-1.52
	ev GW	9.30	9.47	-1.80	-1.54
qs <i>GW</i>		9.40	9.48	-1.75	-1.59
CCSD(T)/CBS ⁶		9.44		-1.53	

S3. VIBRATIONAL FREQUENCIES OF NEUTRAL BENZENE WITHIN DFT AND *GW*

 TABLE S2. Vibrational frequencies (ω) of the a_{1g} and $e_{2g}(\theta)$ normal modes of neutral benzene within DFT and *GW*, calculated as the second derivative of the SCF and Galitski-Migdal total energies respectively. All values are in cm^{-1} .

Functional		$\omega_{1a_{1g}}$	$\omega_{2a_{1g}}$	$\omega_{1e_{2g}(\theta)}$	$\omega_{2e_{2g}(\theta)}$	$\omega_{3e_{2g}(\theta)}$	$\omega_{4e_{2g}(\theta)}$
BLYP	DFT	1010	3208	614	1178	1614	3204
	<i>GW</i>	1024	3240	575	1163	1639	3227
B3LYP	DFT	1015	3196	624	1200	1637	3170
	<i>GW</i>	1026	3247	584	1179	1647	3234
CAM-B3LYP	DFT	1021	3246	633	1209	1659	3242
	<i>GW</i>	1029	3257	598	1204	1661	3244
tCAM-B3LYP	DFT	1014	3230	618	1180	1631	3227
	<i>GW</i>	1030	3258	597	1203	1663	3245
IP-tCAM-B3LYP	DFT	1020	3250	624	1187	1651	3247
	<i>GW</i>	1030	3260	604	1215	1667	3248
CCSD(T)/cc-pVTZ ⁷		1005	3209	607	1189	1637	3181

S4. EFFECT OF THE BASIS SET AND NORMAL MODE COORDINATES

We do not consider the C–H bond stretching modes in this section because of their relative insignificance with respect to the JT effect in the benzene cation and anion.

The effect of the basis set on the computed vibrational frequencies and vibronic coupling constants is given in Tables S3 to S5. It can be seen from Table S3 that the basis set effect on the vibrational frequencies is relatively small compared to the IP and EA of benzene. The largest difference between the def2-TZVPP and def2-QZVPP results is small, about 20 cm^{-1} only. Similarly, the effect on the linear vibronic coupling constants, $V_i^{(+,1)}$ and $V_i^{(-,1)}$, is small (Tables S4 and S5). As suggested in our previous work, the numerical computation of the vibrational frequencies and vibronic coupling constants leads to the basis set errors cancelling each other, and explains the weakened basis set effect here.

TABLE S3. Basis set effect on the vibrational frequencies of neutral benzene within B3LYP and GW . These are computed numerically as the second derivative of the SCF and Galitski-Migdal total energies respectively. All values are in cm^{-1} .

	DFT		GW	
	def2-TZVPP	def2-QZVPP	def2-TZVPP	def2-QZVPP
$\omega_{1a_{1g}}$	1016	1013	1026	1009
$\omega_{1e_{2g}}$	629	629	584	592
$\omega_{2e_{2g}}$	1206	1207	1179	1174
$\omega_{3e_{2g}}$	1643	1639	1647	1635

TABLE S4. Basis set effect on the computed values of $V_i^{(+,1)}$ within B3LYP and G_0W_0 @B3LYP. All values are in 10^{-4} a.u.^{-1} .

	B3LYP		G_0W_0	
	def2-TZVPP	def2-QZVPP	def2-TZVPP	def2-QZVPP
$\omega_{1a_{1g}}$	1.59	1.56	2.08	2.09
$\omega_{1e_{2g}}$	1.47	1.47	1.47	1.46
$\omega_{2e_{2g}}$	2.04	2.04	2.05	2.06
$\omega_{3e_{2g}}$	4.90	4.90	4.88	4.91

TABLE S5. Basis set effect on the computed values of $V_i^{(+,1)}$ within B3LYP and G_0W_0 @B3LYP. All values are in 10^{-4} a.u.^{-1} .

	B3LYP		G_0W_0	
	def2-TZVPP	def2-QZVPP	def2-TZVPP	def2-QZVPP
$\omega_{1a_{1g}}$	3.11	3.09	3.47	3.42
$\omega_{1e_{2g}}$	0.51	0.51	0.55	0.53
$\omega_{2e_{2g}}$	2.51	2.49	2.50	2.46
$\omega_{3e_{2g}}$	5.87	5.74	5.77	5.61

Next, the effect of the normal mode coordinates on the computed vibrational frequencies and linear vibronic coupling constants is given in Tables S6 to S8. We find that the effect of the normal mode coordinates is negligible for the $\nu_{1e_{2g}}$ and $\nu_{2e_{2g}}$ normal modes, and is slightly stronger in the $\nu_{1a_{1g}}$ and $\nu_{3e_{2g}}$ normal modes (Table S6). The effect on the linear vibronic coupling constants is also weak in general, with the strongest effect observed in $V_{3e_{2g}}^{(+,1)}$ (Tables S7 and S8). The Gaussian16 program was used in this set of calculations.

TABLE S6. Effect of the normal mode coordinates on the numerical calculation of the vibrational frequencies, using the normal mode coordinates obtained with the BLYP, B3LYP, and CAM-B3LYP functionals. All values are in cm^{-1} .

	Normal mode coordinates	BLYP	B3LYP	CAM-B3LYP
$\omega_{1a_{1g}}$	B3LYP	1010	1016	1020
	CAM-B3LYP	1026	1031	1036
$\omega_{1e_{2g}}$	B3LYP	609	625	630
	CAM-B3LYP	610	625	630
$\omega_{2e_{2g}}$	B3LYP	1176	1205	1208
	CAM-B3LYP	1180	1209	1213
$\omega_{3e_{2g}}$	B3LYP	1611	1640	1657
	CAM-B3LYP	1632	1660	1677

TABLE S7. Effect of the normal mode coordinates on the computed values of $V_i^{(+,1)}$. The normal mode coordinates were obtained with the BLYP, B3LYP, and CAM-B3LYP functionals. All values are in $10^{-4} \text{ a.u.}^{-1}$.

	Normal mode coordinates	BLYP	B3LYP	CAM-B3LYP
$V_{1a_{1g}}^{(+,1)}$	B3LYP	1.38	1.59	1.81
	CAM-B3LYP	1.39	1.61	1.82
$V_{1e_{2g}}^{(+,1)}$	B3LYP	1.39	1.47	1.50
	CAM-B3LYP	1.40	1.48	1.51
$V_{2e_{2g}}^{(+,1)}$	B3LYP	1.86	2.04	2.20
	CAM-B3LYP	1.80	1.97	2.12
$V_{3e_{2g}}^{(+,1)}$	B3LYP	4.37	4.91	5.24
	CAM-B3LYP	4.45	4.99	5.50

TABLE S8. Effect of the normal mode coordinates on the computed values of $V_i^{(-,1)}$. The normal mode coordinates were obtained with the BLYP, B3LYP, and CAM-B3LYP functionals. All values are in $10^{-4} \text{ a.u.}^{-1}$.

	Normal mode coordinates	BLYP	B3LYP	CAM-B3LYP
$V_{1a_{1g}}^{(+,1)}$	B3LYP	3.00	3.11	3.24
	CAM-B3LYP	3.02	3.13	3.26
$V_{1e_{2g}}^{(+,1)}$	B3LYP	0.45	0.51	0.57
	CAM-B3LYP	0.47	0.53	0.59
$V_{2e_{2g}}^{(+,1)}$	B3LYP	2.38	2.51	2.60
	CAM-B3LYP	2.29	2.42	2.50
$V_{3e_{2g}}^{(+,1)}$	B3LYP	5.59	5.87	6.05
	CAM-B3LYP	5.68	5.96	6.14

S5. VIBRONIC COUPLING CONSTANTS OF BENZENE

TABLE S9. DFT orbital vibronic coupling constants of the frontier orbitals in benzene. The values of $V_i^{(+,1)}$ and $V_i^{(-,1)}$ are the absolute values of the orbital vibronic coupling constants. All results are in 10^{-4} a.u.

Mode		BLYP	B3LYP	CAM-B3LYP	tCAM-B3LYP	IP-tCAM-B3LYP
ν_{1a_1g}	$\langle \psi_{e_{1g}(\theta)} \hat{v}_{1a_1g}^{(1)} \psi_{e_{1g}(\theta)} \rangle$	-1.38	-1.59	-1.81	-1.58	-1.83
	$\langle \psi_{e_{1g}(\epsilon)} \hat{v}_{1a_1g}^{(1)} \psi_{e_{1g}(\epsilon)} \rangle$	-1.38	-1.59	-1.81	-1.58	-1.83
	$\langle \psi_{e_{2u}(\theta)} \hat{v}_{1a_1g}^{(1)} \psi_{e_{2u}(\theta)} \rangle$	3.00	3.11	3.24	3.09	3.25
	$\langle \psi_{e_{2u}(\epsilon)} \hat{v}_{1a_1g}^{(1)} \psi_{e_{2u}(\epsilon)} \rangle$	2.99	3.11	3.23	3.09	3.25
ν_{2a_2g}	$\langle \psi_{e_{1g}(\theta)} \hat{v}_{2a_1g}^{(1)} \psi_{e_{1g}(\theta)} \rangle$	1.85	1.90	1.88	1.73	1.73
	$\langle \psi_{e_{1g}(\epsilon)} \hat{v}_{2a_1g}^{(1)} \psi_{e_{1g}(\epsilon)} \rangle$	1.84	1.90	1.88	1.72	1.73
	$\langle \psi_{e_{2u}(\theta)} \hat{v}_{2a_1g}^{(1)} \psi_{e_{2u}(\theta)} \rangle$	-0.05	-0.19	-0.39	-0.31	-0.53
	$\langle \psi_{e_{2u}(\epsilon)} \hat{v}_{2a_1g}^{(1)} \psi_{e_{2u}(\epsilon)} \rangle$	-0.05	-0.19	-0.40	-0.31	-0.53
$\nu_{1e_{2g}}(\theta)$	$\langle \psi_{e_{1g}(\theta)} \hat{v}_{1e_{2g}(\theta)}^{(1)} \psi_{e_{1g}(\theta)} \rangle$	-1.39	-1.47	-1.50	-1.42	-1.46
	$\langle \psi_{e_{1g}(\epsilon)} \hat{v}_{1e_{2g}(\theta)}^{(1)} \psi_{e_{1g}(\epsilon)} \rangle$	1.39	1.47	1.50	1.42	1.46
	$\langle \psi_{e_{2u}(\theta)} \hat{v}_{1e_{2g}(\theta)}^{(1)} \psi_{e_{2u}(\theta)} \rangle$	-0.46	-0.51	-0.58	-0.53	-0.59
	$\langle \psi_{e_{2u}(\epsilon)} \hat{v}_{1e_{2g}(\theta)}^{(1)} \psi_{e_{2u}(\epsilon)} \rangle$	0.46	0.51	0.57	0.53	0.59
$\nu_{2e_{2g}}(\theta)$	$\langle \psi_{e_{1g}(\theta)} \hat{v}_{2e_{2g}(\theta)}^{(1)} \psi_{e_{1g}(\theta)} \rangle$	-1.86	-2.04	-2.20	-2.03	-2.21
	$\langle \psi_{e_{1g}(\epsilon)} \hat{v}_{2e_{2g}(\theta)}^{(1)} \psi_{e_{1g}(\epsilon)} \rangle$	1.86	2.04	2.20	2.02	2.21
	$\langle \psi_{e_{2u}(\theta)} \hat{v}_{2e_{2g}(\theta)}^{(1)} \psi_{e_{2u}(\theta)} \rangle$	2.38	2.51	2.61	2.47	2.59
	$\langle \psi_{e_{2u}(\epsilon)} \hat{v}_{2e_{2g}(\theta)}^{(1)} \psi_{e_{2u}(\epsilon)} \rangle$	-2.38	-2.51	-2.61	-2.47	-2.59
$\nu_{3e_{2g}}(\theta)$	$\langle \psi_{e_{1g}(\theta)} \hat{v}_{3e_{2g}(\theta)}^{(1)} \psi_{e_{1g}(\theta)} \rangle$	-4.38	-4.91	-5.42	-4.81	-5.40
	$\langle \psi_{e_{1g}(\epsilon)} \hat{v}_{3e_{2g}(\theta)}^{(1)} \psi_{e_{1g}(\epsilon)} \rangle$	4.37	4.90	5.41	4.80	5.39
	$\langle \psi_{e_{2u}(\theta)} \hat{v}_{3e_{2g}(\theta)}^{(1)} \psi_{e_{2u}(\theta)} \rangle$	5.59	5.87	6.06	5.73	5.99
	$\langle \psi_{e_{2u}(\epsilon)} \hat{v}_{3e_{2g}(\theta)}^{(1)} \psi_{e_{2u}(\epsilon)} \rangle$	-5.59	-5.87	-6.06	-5.73	-5.98
$\nu_{4e_{2g}}(\theta)$	$\langle \psi_{e_{1g}(\theta)} \hat{v}_{4e_{2g}(\theta)}^{(1)} \psi_{e_{1g}(\theta)} \rangle$	0.08	0.03	0.05	0.03	0.04
	$\langle \psi_{e_{1g}(\epsilon)} \hat{v}_{4e_{2g}(\theta)}^{(1)} \psi_{e_{1g}(\epsilon)} \rangle$	-0.06	-0.01	-0.03	-0.02	-0.03
	$\langle \psi_{e_{2u}(\theta)} \hat{v}_{4e_{2g}(\theta)}^{(1)} \psi_{e_{2u}(\theta)} \rangle$	1.21	1.27	1.32	1.27	1.33
	$\langle \psi_{e_{2u}(\epsilon)} \hat{v}_{4e_{2g}(\theta)}^{(1)} \psi_{e_{2u}(\epsilon)} \rangle$	-1.20	-1.26	-1.31	-1.25	-1.32

TABLE S10. G_0W_0 orbital vibronic coupling constants of the frontier orbitals in benzene. The values of $V_i^{(+,1)}$ and $V_i^{(-,1)}$ are the absolute values of the orbital vibronic coupling constants. All results are in 10^{-4} a.u.

Mode	$G_0W_0 @$				
	BLYP	B3LYP	CAM-B3LYP	tCAM-B3LYP	IP-tCAM-B3LYP
$\nu_{1a_{1g}}$	$\langle \psi_{e_{1g}(\theta)} \hat{v}_{1a_{1g}}^{(1)} \psi_{e_{1g}(\theta)} \rangle$	-2.17	-2.08	-2.07	-2.09
	$\langle \psi_{e_{1g}(\epsilon)} \hat{v}_{1a_{1g}}^{(1)} \psi_{e_{1g}(\epsilon)} \rangle$	-2.17	-2.08	-2.07	-2.09
	$\langle \psi_{e_{2u}(\theta)} \hat{v}_{1a_{1g}}^{(1)} \psi_{e_{2u}(\theta)} \rangle$	3.45	3.47	3.42	3.37
	$\langle \psi_{e_{2u}(\epsilon)} \hat{v}_{1a_{1g}}^{(1)} \psi_{e_{2u}(\epsilon)} \rangle$	3.44	3.46	3.42	3.37
$\nu_{2a_{1g}}$	$\langle \psi_{e_{1g}(\theta)} \hat{v}_{2a_{1g}}^{(1)} \psi_{e_{1g}(\theta)} \rangle$	0.91	0.98	1.01	0.95
	$\langle \psi_{e_{1g}(\epsilon)} \hat{v}_{2a_{1g}}^{(1)} \psi_{e_{1g}(\epsilon)} \rangle$	0.91	0.98	1.01	0.95
	$\langle \psi_{e_{2u}(\theta)} \hat{v}_{2a_{1g}}^{(1)} \psi_{e_{2u}(\theta)} \rangle$	0.74	0.58	0.31	0.33
	$\langle \psi_{e_{2u}(\epsilon)} \hat{v}_{2a_{1g}}^{(1)} \psi_{e_{2u}(\epsilon)} \rangle$	0.73	0.58	0.30	0.33
$\nu_{1e_{2g}}(\theta)$	$\langle \psi_{e_{1g}(\theta)} \hat{v}_{1e_{2g}(\theta)}^{(1)} \psi_{e_{1g}(\theta)} \rangle$	-1.40	-1.47	-1.53	-1.50
	$\langle \psi_{e_{1g}(\epsilon)} \hat{v}_{1e_{2g}(\theta)}^{(1)} \psi_{e_{1g}(\epsilon)} \rangle$	1.40	1.47	1.53	1.50
	$\langle \psi_{e_{2u}(\theta)} \hat{v}_{1e_{2g}(\theta)}^{(1)} \psi_{e_{2u}(\theta)} \rangle$	-0.53	-0.55	-0.57	-0.56
	$\langle \psi_{e_{2u}(\epsilon)} \hat{v}_{1e_{2g}(\theta)}^{(1)} \psi_{e_{2u}(\epsilon)} \rangle$	0.53	0.55	0.56	0.57
$\nu_{2e_{2g}}(\theta)$	$\langle \psi_{e_{1g}(\theta)} \hat{v}_{2e_{2g}(\theta)}^{(1)} \psi_{e_{1g}(\theta)} \rangle$	-1.96	-2.05	-2.16	-2.16
	$\langle \psi_{e_{1g}(\epsilon)} \hat{v}_{2e_{2g}(\theta)}^{(1)} \psi_{e_{1g}(\epsilon)} \rangle$	1.95	2.05	2.16	2.16
	$\langle \psi_{e_{2u}(\theta)} \hat{v}_{2e_{2g}(\theta)}^{(1)} \psi_{e_{2u}(\theta)} \rangle$	2.42	2.50	2.57	2.56
	$\langle \psi_{e_{2u}(\epsilon)} \hat{v}_{2e_{2g}(\theta)}^{(1)} \psi_{e_{2u}(\epsilon)} \rangle$	-2.42	-2.50	-2.57	-2.56
$\nu_{3e_{2g}}(\theta)$	$\langle \psi_{e_{1g}(\theta)} \hat{v}_{3e_{2g}(\theta)}^{(1)} \psi_{e_{1g}(\theta)} \rangle$	-4.61	-4.90	-5.20	-5.17
	$\langle \psi_{e_{1g}(\epsilon)} \hat{v}_{3e_{2g}(\theta)}^{(1)} \psi_{e_{1g}(\epsilon)} \rangle$	4.59	4.88	5.18	5.15
	$\langle \psi_{e_{2u}(\theta)} \hat{v}_{3e_{2g}(\theta)}^{(1)} \psi_{e_{2u}(\theta)} \rangle$	5.62	5.77	5.89	5.86
	$\langle \psi_{e_{2u}(\epsilon)} \hat{v}_{3e_{2g}(\theta)}^{(1)} \psi_{e_{2u}(\epsilon)} \rangle$	-5.61	-5.76	-5.88	-5.85
$\nu_{4e_{2g}}(\theta)$	$\langle \psi_{e_{1g}(\theta)} \hat{v}_{4e_{2g}(\theta)}^{(1)} \psi_{e_{1g}(\theta)} \rangle$	0.21	0.16	0.14	0.18
	$\langle \psi_{e_{1g}(\epsilon)} \hat{v}_{4e_{2g}(\theta)}^{(1)} \psi_{e_{1g}(\epsilon)} \rangle$	-0.20	-0.15	-0.16	-0.17
	$\langle \psi_{e_{2u}(\theta)} \hat{v}_{4e_{2g}(\theta)}^{(1)} \psi_{e_{2u}(\theta)} \rangle$	1.17	1.18	1.21	1.23
	$\langle \psi_{e_{2u}(\epsilon)} \hat{v}_{4e_{2g}(\theta)}^{(1)} \psi_{e_{2u}(\epsilon)} \rangle$	-1.15	-1.16	-1.20	-1.21

TABLE S11. ev GW_0 orbital vibronic coupling constants of the frontier orbitals in benzene. The values of $V_i^{(+,1)}$ and $V_i^{(-,1)}$ are the absolute values of the orbital vibronic coupling constants. All results are in 10^{-4} a.u.

Mode	ev GW_0 @				
	BLYP	B3LYP	CAM-B3LYP	tCAM-B3LYP	IP-tCAM-B3LYP
$\nu_{1a_{1g}}$	$\langle \psi_{e_{1g}(\theta)} \hat{v}_{1a_{1g}}^{(1)} \psi_{e_{1g}(\theta)} \rangle$	-2.17	-2.10	-2.10	-2.16
	$\langle \psi_{e_{1g}(\epsilon)} \hat{v}_{1a_{1g}}^{(1)} \psi_{e_{1g}(\epsilon)} \rangle$	-2.17	-2.10	-2.11	-2.16
	$\langle \psi_{e_{2u}(\theta)} \hat{v}_{1a_{1g}}^{(1)} \psi_{e_{2u}(\theta)} \rangle$	3.42	3.44	3.37	3.35
	$\langle \psi_{e_{2u}(\epsilon)} \hat{v}_{1a_{1g}}^{(1)} \psi_{e_{2u}(\epsilon)} \rangle$	3.42	3.44	3.38	3.35
$\nu_{2a_{1g}}$	$\langle \psi_{e_{1g}(\theta)} \hat{v}_{2a_{1g}}^{(1)} \psi_{e_{1g}(\theta)} \rangle$	0.98	1.00	0.97	0.89
	$\langle \psi_{e_{1g}(\epsilon)} \hat{v}_{2a_{1g}}^{(1)} \psi_{e_{1g}(\epsilon)} \rangle$	0.99	1.00	0.97	0.89
	$\langle \psi_{e_{2u}(\theta)} \hat{v}_{2a_{1g}}^{(1)} \psi_{e_{2u}(\theta)} \rangle$	0.60	0.48	0.32	0.29
	$\langle \psi_{e_{2u}(\epsilon)} \hat{v}_{2a_{1g}}^{(1)} \psi_{e_{2u}(\epsilon)} \rangle$	0.58	0.47	0.32	0.25
$\nu_{1e_{2g}}(\theta)$	$\langle \psi_{e_{1g}(\theta)} \hat{v}_{1e_{2g}(\theta)}^{(1)} \psi_{e_{1g}(\theta)} \rangle$	-1.44	-1.51	-1.54	-1.51
	$\langle \psi_{e_{1g}(\epsilon)} \hat{v}_{1e_{2g}(\theta)}^{(1)} \psi_{e_{1g}(\epsilon)} \rangle$	1.47	1.49	1.53	1.53
	$\langle \psi_{e_{2u}(\theta)} \hat{v}_{1e_{2g}(\theta)}^{(1)} \psi_{e_{2u}(\theta)} \rangle$	-0.54	-0.58	-0.58	-0.57
	$\langle \psi_{e_{2u}(\epsilon)} \hat{v}_{1e_{2g}(\theta)}^{(1)} \psi_{e_{2u}(\epsilon)} \rangle$	0.55	0.56	0.55	0.56
$\nu_{2e_{2g}}(\theta)$	$\langle \psi_{e_{1g}(\theta)} \hat{v}_{2e_{2g}(\theta)}^{(1)} \psi_{e_{1g}(\theta)} \rangle$	-2.11	-2.14	-2.17	-2.19
	$\langle \psi_{e_{1g}(\epsilon)} \hat{v}_{2e_{2g}(\theta)}^{(1)} \psi_{e_{1g}(\epsilon)} \rangle$	2.10	2.12	2.18	2.19
	$\langle \psi_{e_{2u}(\theta)} \hat{v}_{2e_{2g}(\theta)}^{(1)} \psi_{e_{2u}(\theta)} \rangle$	2.51	2.50	2.59	2.56
	$\langle \psi_{e_{2u}(\epsilon)} \hat{v}_{2e_{2g}(\theta)}^{(1)} \psi_{e_{2u}(\epsilon)} \rangle$	-2.52	-2.56	-2.57	-2.59
$\nu_{3e_{2g}}(\theta)$	$\langle \psi_{e_{1g}(\theta)} \hat{v}_{3e_{2g}(\theta)}^{(1)} \psi_{e_{1g}(\theta)} \rangle$	-5.04	-5.13	-5.23	-5.25
	$\langle \psi_{e_{1g}(\epsilon)} \hat{v}_{3e_{2g}(\theta)}^{(1)} \psi_{e_{1g}(\epsilon)} \rangle$	5.02	5.09	5.22	5.24
	$\langle \psi_{e_{2u}(\theta)} \hat{v}_{3e_{2g}(\theta)}^{(1)} \psi_{e_{2u}(\theta)} \rangle$	5.83	5.87	5.89	5.88
	$\langle \psi_{e_{2u}(\epsilon)} \hat{v}_{3e_{2g}(\theta)}^{(1)} \psi_{e_{2u}(\epsilon)} \rangle$	-5.83	-5.88	-5.91	-5.91
$\nu_{4e_{2g}}(\theta)$	$\langle \psi_{e_{1g}(\theta)} \hat{v}_{4e_{2g}(\theta)}^{(1)} \psi_{e_{1g}(\theta)} \rangle$	0.21	0.16	0.16	0.19
	$\langle \psi_{e_{1g}(\epsilon)} \hat{v}_{4e_{2g}(\theta)}^{(1)} \psi_{e_{1g}(\epsilon)} \rangle$	-0.18	-0.13	-0.15	-0.18
	$\langle \psi_{e_{2u}(\theta)} \hat{v}_{4e_{2g}(\theta)}^{(1)} \psi_{e_{2u}(\theta)} \rangle$	1.23	1.24	1.23	1.25
	$\langle \psi_{e_{2u}(\epsilon)} \hat{v}_{4e_{2g}(\theta)}^{(1)} \psi_{e_{2u}(\epsilon)} \rangle$	-1.20	-1.18	-1.20	-1.24

TABLE S12. ev GW and qs GW orbital vibronic coupling constants of the frontier orbitals in benzene. B3LYP was used as the mean-field method to start the qs GW calculations. The values of $V_i^{(+,1)}$ and $V_i^{(-,1)}$ are the absolute values of the orbital vibronic coupling constants. All results are in 10^{-4} a.u.

Mode		ev GW @					qs GW B3LYP
		BLYP	B3LYP	CAM-B3LYP	tCAM-B3LYP	IP-tCAM-B3LYP	
ν_{1a_1g}	$\langle \psi_{e_{1g}(\theta)} \hat{v}_{1a_1g}^{(1)} \psi_{e_{1g}(\theta)} \rangle$	-2.20	-2.11	-2.11	-2.13	-2.12	-2.16
	$\langle \psi_{e_{1g}(\epsilon)} \hat{v}_{1a_1g}^{(1)} \psi_{e_{1g}(\epsilon)} \rangle$	-2.21	-2.11	-2.11	-2.13	-2.12	-2.16
	$\langle \psi_{e_{2u}(\theta)} \hat{v}_{1a_1g}^{(1)} \psi_{e_{2u}(\theta)} \rangle$	3.37	3.45	3.44	3.41	3.43	3.44
	$\langle \psi_{e_{2u}(\epsilon)} \hat{v}_{1a_1g}^{(1)} \psi_{e_{2u}(\epsilon)} \rangle$	3.37	3.45	3.43	3.41	3.43	3.44
ν_{2a_1g}	$\langle \psi_{e_{1g}(\theta)} \hat{v}_{2a_1g}^{(1)} \psi_{e_{1g}(\theta)} \rangle$	1.17	1.14	1.04	0.99	0.89	1.32
	$\langle \psi_{e_{1g}(\epsilon)} \hat{v}_{2a_1g}^{(1)} \psi_{e_{1g}(\epsilon)} \rangle$	1.17	1.13	1.04	1.00	0.89	1.32
	$\langle \psi_{e_{2u}(\theta)} \hat{v}_{2a_1g}^{(1)} \psi_{e_{2u}(\theta)} \rangle$	0.46	0.40	0.27	0.30	0.34	0.47
	$\langle \psi_{e_{2u}(\epsilon)} \hat{v}_{2a_1g}^{(1)} \psi_{e_{2u}(\epsilon)} \rangle$	0.45	0.40	0.26	0.29	0.36	0.47
$\nu_{1e_2g}(\theta)$	$\langle \psi_{e_{1g}(\theta)} \hat{v}_{1e_2g}^{(1)} \psi_{e_{1g}(\theta)} \rangle$	-1.50	-1.53	-1.57	-1.52	-1.54	-1.55
	$\langle \psi_{e_{1g}(\epsilon)} \hat{v}_{1e_2g}^{(1)} \psi_{e_{1g}(\epsilon)} \rangle$	1.53	1.52	1.55	1.53	1.54	1.54
	$\langle \psi_{e_{2u}(\theta)} \hat{v}_{1e_2g}^{(1)} \psi_{e_{2u}(\theta)} \rangle$	-0.55	-0.58	-0.58	-0.57	-0.57	-0.47
	$\langle \psi_{e_{2u}(\epsilon)} \hat{v}_{1e_2g}^{(1)} \psi_{e_{2u}(\epsilon)} \rangle$	0.59	0.57	0.57	0.57	0.57	0.47
$\nu_{2e_2g}(\theta)$	$\langle \psi_{e_{1g}(\theta)} \hat{v}_{2e_2g}^{(1)} \psi_{e_{1g}(\theta)} \rangle$	-2.24	-2.22	-2.22	-2.23	-2.23	-2.20
	$\langle \psi_{e_{1g}(\epsilon)} \hat{v}_{2e_2g}^{(1)} \psi_{e_{1g}(\epsilon)} \rangle$	2.23	2.22	2.21	2.21	2.20	2.20
	$\langle \psi_{e_{2u}(\theta)} \hat{v}_{2e_2g}^{(1)} \psi_{e_{2u}(\theta)} \rangle$	2.57	2.60	2.59	2.60	2.58	2.62
	$\langle \psi_{e_{2u}(\epsilon)} \hat{v}_{2e_2g}^{(1)} \psi_{e_{2u}(\epsilon)} \rangle$	-2.62	-2.59	-2.59	-2.59	-2.61	-2.62
$\nu_{3e_2g}(\theta)$	$\langle \psi_{e_{1g}(\theta)} \hat{v}_{3e_2g}^{(1)} \psi_{e_{1g}(\theta)} \rangle$	-5.36	-5.32	-5.32	-5.32	-5.28	-5.47
	$\langle \psi_{e_{1g}(\epsilon)} \hat{v}_{3e_2g}^{(1)} \psi_{e_{1g}(\epsilon)} \rangle$	5.35	5.32	5.30	5.32	5.30	5.49
	$\langle \psi_{e_{2u}(\theta)} \hat{v}_{3e_2g}^{(1)} \psi_{e_{2u}(\theta)} \rangle$	5.99	5.98	5.94	5.94	5.91	6.10
	$\langle \psi_{e_{2u}(\epsilon)} \hat{v}_{3e_2g}^{(1)} \psi_{e_{2u}(\epsilon)} \rangle$	-5.96	-5.94	-5.92	-5.92	-5.90	-6.06
$\nu_{4e_2g}(\theta)$	$\langle \psi_{e_{1g}(\theta)} \hat{v}_{4e_2g}^{(1)} \psi_{e_{1g}(\theta)} \rangle$	0.19	0.14	0.15	0.12	0.16	0.09
	$\langle \psi_{e_{1g}(\epsilon)} \hat{v}_{4e_2g}^{(1)} \psi_{e_{1g}(\epsilon)} \rangle$	-0.18	-0.13	-0.15	-0.15	-0.17	-0.10
	$\langle \psi_{e_{2u}(\theta)} \hat{v}_{4e_2g}^{(1)} \psi_{e_{2u}(\theta)} \rangle$	1.29	1.25	1.24	1.27	1.24	1.26
	$\langle \psi_{e_{2u}(\epsilon)} \hat{v}_{4e_2g}^{(1)} \psi_{e_{2u}(\epsilon)} \rangle$	-1.30	-1.23	-1.22	-1.23	-1.24	-1.26

TABLE S13. DFT and GW dimensionless linear vibronic coupling constants of the benzene cation, $D_i^{(+,1)} = V_i^{(+,1)} / \sqrt{\hbar\omega_i^3}$, where $\omega_i^{\text{DFT}/\text{GW}}$ is the vibrational frequency of normal mode i within DFT/GW. The values of $D_i^{(+,1)}$ calculated using the GW result for $V_i^{(+,1)}$ and the GW vibrational frequencies ω_i^{DFT} is also given in parentheses. The B3LYP vibrational frequencies were used in the case of qs GW .

This work		$D_{1a_{1g}}^{(+,1)}$	$D_{2a_{1g}}^{(+,1)}$	$D_{1e_{2g}}^{(+,1)}$	$D_{2e_{2g}}^{(+,1)}$	$D_{3e_{2g}}^{(+,1)}$	$D_{4e_{2g}}^{(+,1)}$
BLYP	DFT	0.224	0.104	0.941	0.474	0.693	0.004
	G_0W_0	0.694 (0.680)	0.052 (0.051)	0.946 (1.045)	0.497 (0.506)	0.727 (0.711)	0.011 (0.011)
	ev GW_0	0.702 (0.688)	0.057 (0.056)	0.993 (1.097)	0.535 (0.546)	0.796 (0.777)	0.010 (0.009)
	ev GW	0.705 (0.690)	0.067 (0.066)	1.024 (1.131)	0.569 (0.580)	0.850 (0.831)	0.010 (0.010)
B3LYP	DFT	0.506	0.108	0.968	0.504	0.761	0.001
	G_0W_0	0.661 (0.650)	0.056 (0.055)	0.969 (1.070)	0.507 (0.520)	0.757 (0.750)	0.008 (0.008)
	ev GW_0	0.665 (0.654)	0.058 (0.056)	0.984 (1.087)	0.524 (0.538)	0.794 (0.787)	0.008 (0.008)
	ev GW	0.673 (0.662)	0.065 (0.063)	1.006 (1.111)	0.550 (0.564)	0.829 (0.821)	0.007 (0.007)
CAM-B3LYP	DFT	0.571	0.105	0.969	0.539	0.824	0.002
	G_0W_0	0.654 (0.646)	0.056 (0.056)	0.989 (1.076)	0.527 (0.531)	0.788 (0.787)	0.009 (0.009)
	ev GW_0	0.664 (0.656)	0.054 (0.054)	1.006 (1.094)	0.530 (0.534)	0.797 (0.796)	0.008 (0.008)
	ev GW	0.663 (0.655)	0.057 (0.056)	0.992 (1.079)	0.540 (0.543)	0.807 (0.806)	0.008 (0.008)
tCAM-B3LYP	DFT	0.503	0.097	0.953	0.513	0.750	0.001
	G_0W_0	0.666 (0.651)	0.053 (0.053)	1.008 (1.060)	0.548 (0.533)	0.804 (0.781)	0.009 (0.009)
	ev GW_0	0.686 (0.671)	0.054 (0.053)	1.021 (1.074)	0.558 (0.542)	0.818 (0.794)	0.009 (0.009)
	ev GW	0.681 (0.667)	0.056 (0.055)	1.024 (1.077)	0.563 (0.547)	0.830 (0.806)	0.009 (0.009)
IP-tCAM-B3LYP	DFT	0.578	0.096	0.965	0.556	0.827	0.002
	G_0W_0	0.664 (0.654)	0.052 (0.051)	1.019 (1.069)	0.555 (0.537)	0.810 (0.780)	0.009 (0.009)
	ev GW_0	0.667 (0.657)	0.049 (0.049)	1.011 (1.060)	0.555 (0.536)	0.805 (0.775)	0.009 (0.009)
	ev GW	0.669 (0.659)	0.050 (0.049)	1.019 (1.069)	0.554 (0.535)	0.810 (0.780)	0.009 (0.009)
qs GW		0.688	0.075	1.017	0.543	0.849	0.006

TABLE S14. DFT and GW dimensionless linear vibronic coupling constants of the benzene anion, $D_i^{(-,1)} = V_i^{(-,1)} / \sqrt{\hbar\omega_i^3}$, where $\omega_i^{\text{DFT}/\text{GW}}$ is the vibrational frequency of normal mode i within DFT/ GW . The values of $D_i^{(-,1)}$ calculated using the GW result for $V_i^{(-,1)}$ and the DFT vibrational frequencies ω_i^{DFT} is given in parentheses. The B3LYP vibrational frequencies were used in the case of $\text{qs}GW$.

This work		$D_{1a_{1g}}^{(-,1)}$	$D_{2a_{1g}}^{(-,1)}$	$D_{1e_{2g}}^{(-,1)}$	$D_{2e_{2g}}^{(-,1)}$	$D_{3e_{2g}}^{(-,1)}$	$D_{4e_{2g}}^{(-,1)}$
BLYP	DFT	0.959	0.003	0.309	0.607	0.886	0.068
	G_0W_0	1.103 (1.081)	0.042 (0.041)	0.357 (0.394)	0.616 (0.627)	0.890 (0.870)	0.066 (0.066)
	ev GW_0	1.085 (1.063)	0.034 (0.033)	0.358 (0.396)	0.635 (0.647)	0.923 (0.902)	0.071 (0.070)
	ev GW	1.075 (1.053)	0.027 (0.026)	0.385 (0.425)	0.657 (0.670)	0.948 (0.926)	0.074 (0.073)
B3LYP	DFT	0.988	0.011	0.338	0.622	0.911	0.073
	G_0W_0	1.102 (1.084)	0.033 (0.032)	0.362 (0.400)	0.617 (0.634)	0.896 (0.887)	0.068 (0.066)
	ev GW_0	1.080 (1.080)	0.027 (0.026)	0.387 (0.427)	0.629 (0.645)	0.915 (0.907)	0.070 (0.068)
	ev GW	1.092 (1.074)	0.023 (0.023)	0.379 (0.419)	0.645 (0.662)	0.929 (0.921)	0.070 (0.070)
CAM-B3LYP	DFT	1.020	0.022	0.372	0.637	0.922	0.074
	G_0W_0	1.077 (1.065)	0.017 (0.017)	0.365 (0.397)	0.628 (0.633)	0.896 (0.894)	0.068 (0.068)
	ev GW_0	1.067 (1.055)	0.017 (0.017)	0.354 (0.385)	0.628 (0.632)	0.898 (0.897)	0.067 (0.067)
	ev GW	1.088 (1.075)	0.014 (0.014)	0.375 (0.408)	0.636 (0.641)	0.903 (0.902)	0.069 (0.069)
tCAM-B3LYP	DFT	0.984	0.018	0.354	0.628	0.894	0.071
	G_0W_0	(1.0501.074)	0.018 (0.018)	0.375 (0.394)	0.649 (0.631)	0.915 (0.889)	0.069 (0.068)
	ev GW_0	1.067 (1.044)	0.019 (0.019)	0.385 (0.405)	0.655 (0.636)	0.919 (0.893)	0.071 (0.071)
	ev GW	1.084 (1.060)	0.016 (0.016)	0.384 (0.404)	0.657 (0.639)	0.926 (0.899)	0.071 (0.070)
IP-tCAM-B3LYP	DFT	1.026	0.029	0.392	0.652	0.918	0.074
	G_0W_0	1.065 (1.049)	0.007 (0.007)	0.374 (0.392)	0.653 (0.631)	0.906 (0.872)	0.069 (0.069)
	ev GW_0	1.074 (1.058)	0.007 (0.016)	0.375 (0.393)	0.652 (0.630)	0.904 (0.871)	0.068 (0.068)
	ev GW	1.085 (1.069)	0.009 (0.019)	0.374 (0.392)	0.648 (0.626)	0.905 (0.872)	0.069 (0.069)
qs GW		1.095	0.027	0.368	0.648	0.947	0.073

S6. SECOND ORDER VIBRONIC COUPLING

The expansion of the vibronic coupling model to include the second order coupling in the a_{1g} and e_{2g} normal modes is roughly discussed here. As per the main text, we will demonstrate the theory with the cation. The procedure will be the same for the anion. We do not consider intermode coupling in the vibronic Hamiltonian.

The quadratic vibronic Hamiltonian is then

$$H_{vib.} = H^{(0)} + \sum_i V_i^{(1)} Q_i + \frac{1}{2} \sum_{i_1} V_{i_1}^{(2)} Q_{i_1}^2. \quad (4)$$

The simpler a_{1g} case is discussed first. For the a_{1g} normal modes, the second order vibronic Hamiltonian is

$$H_{vib.}(Q_{a_{1g}}) = H^{(0)} + V_{a_{1g}}^{(1)} Q_{a_{1g}} + \frac{V_{a_{1g}}^{(2)}}{2} Q_{a_{1g}}^2. \quad (5)$$

As done for the linear case, the corresponding terms for the neutral molecule, which are just the vibrational frequencies in the case of the second order terms, are used to derive $V_{a_{1g}}^{(2)}$.

$$\begin{aligned} V_{a_{1g}}^{(2)} &= \sum_m n_m \langle \psi_m | \hat{v}_{a_{1g}}^{(2)} | \psi_m \rangle + \frac{\partial^2 U_{nn}}{\partial Q_{a_{1g}}^2} \\ &= \langle \Psi_0 | \hat{V}_{a_{1g}}^{(2)} | \Psi_0 \rangle - \langle \psi_{e_{1g}(\theta)} | \hat{v}_{a_{1g}}^{(2)} | \psi_{e_{1g}(\theta)} \rangle \\ &= \omega_{a_{1g}}^2 - \langle \psi_{e_{1g}(\theta)} | \hat{v}_{a_{1g}}^{(2)} | \psi_{e_{1g}(\theta)} \rangle \end{aligned} \quad (6)$$

where ω is the vibrational frequency of the neutral molecule.

The procedure for the e_{2g} normal modes is more complicated because of the quadratic JT effect. First, the second order vibronic coupling constants of the e_{2g} normal modes can be symmetrized by considering the symmetric product,

$$E_{2g} \otimes E_{2g} = A_{1g} \otimes E_{2g}. \quad (7)$$

The second order vibronic coupling terms for the e_{2g} normal modes can then be grouped into symmetrized combinations as

$$\begin{aligned} \sum_{e_{2g}(\theta)} \sum_{e_{2g}(\epsilon)} V_{e_{2g}(\theta)e_{2g}(\epsilon)}^{(2)} Q_{e_{2g}(\theta)} Q_{e_{2g}(\epsilon)} &= \frac{V_{a'_{1g}}^{(2)}}{2} \left(\frac{1}{\sqrt{2}} (Q_{e_{2g}(\theta)}^2 + Q_{e_{2g}(\epsilon)}^2) \right) \\ &\quad + \frac{V_{e_{2g}(\theta)}^{(2)}}{2} \left(\frac{1}{\sqrt{2}} (Q_{e_{2g}(\theta)}^2 - Q_{e_{2g}(\epsilon)}^2) \right) \\ &\quad - \frac{V_{e_{2g}(\epsilon)}^{(2)}}{2} (\sqrt{2} Q_{e_{2g}(\theta)} Q_{e_{2g}(\epsilon)}) \end{aligned} \quad (8)$$

The prime symbol is used here to distinguish between the a_{1g} component of the second order coupling in the e_{2g} normal modes and the second order coupling for the a_{1g} modes. Including the linear vibronic coupling term, the Hamiltonian for the distortion along a $e_{2g}(\theta)$ normal mode is then

$$H_{vib.}(Q_{e_{2g}(\theta)}) = H^{(0)} + V_{e_{2g}(\theta)}^{(1)} Q_{e_{2g}(\theta)} + \frac{V_{a'_{1g}}^{(2)}}{2} \frac{1}{\sqrt{2}} Q_{e_{2g}(\theta)}^2 + \frac{V_{e_{2g}(\theta)}^{(2)}}{2} \frac{1}{\sqrt{2}} Q_{e_{2g}(\theta)}^2. \quad (9)$$

The matrix representation in the degenerate electronic states of the benzene cation is

$$\begin{aligned} \mathbf{V}_{e_{2g}(\theta)} &= \mathbf{V}_{e_{2g}(\theta)}^{(1)} + \mathbf{V}_{a'_{1g}}^{(2)} + \mathbf{V}_{e_{2g}(\theta)}^{(2)} \\ &= \begin{pmatrix} V_{e_{2g}(\theta)}^{(1)} Q_{e_{2g}(\theta)} & 0 \\ 0 & -V_{e_{2g}(\theta)}^{(1)} Q_{e_{2g}(\theta)} \end{pmatrix} + \begin{pmatrix} \frac{V_{a'_{1g}}^{(2)} Q_{e_{2g}(\theta)}^2}{2\sqrt{2}} & 0 \\ 0 & \frac{V_{a'_{1g}}^{(2)} Q_{e_{2g}(\theta)}^2}{2\sqrt{2}} \end{pmatrix} + \begin{pmatrix} \frac{V_{e_{2g}(\theta)}^{(2)} Q_{e_{2g}(\theta)}^2}{2\sqrt{2}} & 0 \\ 0 & -\frac{V_{e_{2g}(\theta)}^{(2)} Q_{e_{2g}(\theta)}^2}{2\sqrt{2}} \end{pmatrix} \end{aligned} \quad (10)$$

Diagonalising Equation (10), the expression for the PES along a e_{2g} normal mode is

$$E_{\pm}^{(2)}(Q_{e_{2g}(\theta)}) = \pm V_{e_{2g}(\theta)}^{(1)} Q_{e_{2g}(\theta)} + \frac{V_{a'_{1g}}^{(2)} Q_{e_{2g}(\theta)}^2}{2\sqrt{2}} \pm \frac{V_{e_{2g}(\theta)}^{(2)} Q_{e_{2g}(\theta)}^2}{2\sqrt{2}} \quad (11)$$

Hence, the difference between the linear and quadratic vibronic coupling models is the additional $\pm V_{e_{2g}(\theta)}^{(2)} Q_{e_{2g}(\theta)}^2 / 2\sqrt{2}$ term. This term gives rise to the quadratic JT effect, and is used to explain the difference in the energies of the respective JT distorted geometries, as well as the pseudorotation barrier.

Next, the second order terms, $V_{a'_{1g}}^{(2)}$ and $V_{e_{2g}(\theta)}^{(2)}$, will be derived in terms of orbital vibronic coupling constants. As was done for the linear vibronic coupling model, the $V_{e_{2g}(\theta)}^{(2)}$ term can be reduced to a single orbital vibronic coupling constant,

$$V_{e_{2g}(\theta)}^{(2)} = \langle \psi_{e_{1g}(\epsilon)} | \hat{v}_{e_{2g}}^{(2)} | \psi_{e_{1g}(\epsilon)} \rangle \quad (12)$$

However, unlike the linear term, the second order term is not equal to the second derivative of the orbital energies because of the $V_{a'_{1g}}$ term:

$$\frac{\partial^2 \varepsilon_{e_{1g}(\epsilon)}}{\partial Q_{e_{2g}(\theta)}^2} = \langle \psi_{e_{1g}(\epsilon)} | \hat{v}_{a'_{1g}}^{(2)} | \psi_{e_{1g}(\epsilon)} \rangle + \langle \psi_{e_{1g}(\epsilon)} | \hat{v}_{e_{2g}}^{(2)} | \psi_{e_{1g}(\epsilon)} \rangle \quad (13)$$

By the Wigner-Eckart theorem, the second derivative of the other orbital in the degenerate pair can be written as

$$\begin{aligned} \frac{\partial^2 \varepsilon_{e_{1g}(\theta)}}{\partial Q_{e_{2g}(\theta)}^2} &= \langle \psi_{e_{1g}(\theta)} | \hat{v}_{a'_{1g}}^{(2)} | \psi_{e_{1g}(\theta)} \rangle + \langle \psi_{e_{1g}(\theta)} | \hat{v}_{e_{2g}}^{(2)} | \psi_{e_{1g}(\theta)} \rangle \\ &= \langle \psi_{e_{1g}(\epsilon)} | \hat{v}_{a'_{1g}}^{(2)} | \psi_{e_{1g}(\epsilon)} \rangle - \langle \psi_{e_{1g}(\epsilon)} | \hat{v}_{e_{2g}}^{(2)} | \psi_{e_{1g}(\epsilon)} \rangle \end{aligned} \quad (14)$$

Combining Equations (13) and (14), $V_{e_{2g}(\theta)}^{(2)}$ becomes:

$$V_{e_{2g}(\theta)}^{(2)} = \frac{1}{2} \left(\frac{\partial^2 \varepsilon_{e_{1g}(\epsilon)}}{\partial Q_{e_{2g}(\theta)}^2} - \frac{\partial^2 \varepsilon_{e_{1g}(\theta)}}{\partial Q_{e_{2g}(\theta)}^2} \right) \quad (15)$$

and we also get

$$\langle \psi_{e_{1g}(\theta)} | \hat{v}_{a'_{1g}}^{(2)} | \psi_{e_{1g}(\theta)} \rangle = \frac{1}{2} \left(\frac{\partial^2 \varepsilon_{e_{1g}(\epsilon)}}{\partial Q_{e_{2g}(\theta)}^2} + \frac{\partial^2 \varepsilon_{e_{1g}(\theta)}}{\partial Q_{e_{2g}(\theta)}^2} \right) \quad (16)$$

Similar to the procedure for the a_{1g} normal modes, the second order $V_{a'_{1g}}^{(2)}$ terms for the e_{2g} modes will be derived using the vibrational frequencies of the neutral molecule.

$$\begin{aligned} V_{a'_{1g}}^{(2)} &= \sum_m n_m \langle \psi_m | \hat{v}_{a'_{1g}}^{(2)} | \psi_m \rangle + \frac{\partial^2 U_{nn}}{\partial Q_{e_{2g}}^2} \\ &= \langle \Psi_0 | \hat{V}_{e_{2g}}^{(2)} | \Psi_0 \rangle - \langle \psi_{e_{1g}(\theta)} | \hat{v}_{a'_{1g}}^{(2)} | \psi_{e_{1g}(\theta)} \rangle \\ &= \omega_{e_{2g}}^2 - \langle \psi_{e_{1g}(\theta)} | \hat{v}_{a'_{1g}}^{(2)} | \psi_{e_{1g}(\theta)} \rangle \\ &= \omega_{e_{2g}}^2 - \frac{1}{2} \left(\frac{\partial^2 \varepsilon_{e_{1g}(\epsilon)}}{\partial Q_{e_{2g}(\theta)}^2} + \frac{\partial^2 \varepsilon_{e_{1g}(\theta)}}{\partial Q_{e_{2g}(\theta)}^2} \right) \end{aligned} \quad (17)$$

Lastly, the vibrational frequencies for the e_{2g} normal modes (ω') in the two degenerate electronic states of the benzene cation can be calculated as

$$\begin{aligned} |E_{1g}(\theta)\rangle : \omega'_{e_{2g}}^2 &= \frac{1}{\sqrt{2}} \left(V_{a'_{1g}}^{(2)} + V_{e_{2g}(\theta)}^{(2)} \right) \\ &= \omega_{e_{2g}}^2 - \frac{\partial^2 \varepsilon_{e_{1g}(\theta)}}{\partial Q_{e_{2g}(\theta)}^2} \end{aligned} \quad (18a)$$

$$\begin{aligned}
|E_{1g}(\epsilon)\rangle : \omega'_{e_{2g}}^2 &= \frac{1}{\sqrt{2}} \left(V_{a'_{1g}}^{(2)} - V_{e_{2g}(\theta)}^{(2)} \right) \\
&= \omega_{e_{2g}}^2 - \frac{\partial^2 \varepsilon_{e_{1g}(\epsilon)}}{\partial Q_{e_{2g}(\theta)}^2}
\end{aligned} \tag{18b}$$

The raw computational results is given in Table S15 below. Only the ev GW results are given for brevity. A comparison of the vibrational frequencies of neutral benzene and the radical cation/anion calculated using Equations (18a) and (18b) is given in Table S16.

TABLE S15. Second order derivatives of the ev GW quasiparticle energies ($\varepsilon''_{e_{1g}(\theta)}$ and $\varepsilon''_{e_{1g}(\epsilon)}$)

Mode		ev GW @				
		BLYP	B3LYP	CAM-B3LYP	tCAM-B3LYP	IP-tCAM-B3LYP
$\nu_{1a_{1g}}$	$\varepsilon''_{e_{1g}(\theta)}$	-9.36E-08	-5.77E-07	-4.37E-07	-4.44E-07	-3.15E-07
	$\varepsilon''_{e_{1g}(\epsilon)}$	-1.44E-07	-5.40E-07	-4.51E-07	-4.87E-07	-2.92E-07
	$\varepsilon''_{e_{2u}(\theta)}$	8.76E-07	2.36E-07	7.48E-07	6.90E-07	6.62E-07
	$\varepsilon''_{e_{2u}(\epsilon)}$	9.73E-07	2.46E-07	6.80E-07	6.44E-07	7.17E-07
$\nu_{2a_{1g}}$	$\varepsilon''_{e_{1g}(\theta)}$	-2.07E-06	-2.22E-06	-1.95E-06	-2.35E-06	-2.24E-06
	$\varepsilon''_{e_{1g}(\epsilon)}$	-2.01E-06	-2.23E-06	-2.00E-06	-2.35E-06	-2.24E-06
	$\varepsilon''_{e_{2u}(\theta)}$	-1.73E-06	-2.05E-06	-1.82E-06	-2.10E-06	-4.09E-07
	$\varepsilon''_{e_{2u}(\epsilon)}$	-1.82E-06	-2.08E-06	-1.91E-06	-2.10E-06	-2.21E-07
$\nu_{1e_{2g}(\theta)}$	$\varepsilon''_{e_{1g}(\theta)}$	1.20E-07	5.64E-07	8.39E-07	8.81E-07	4.24E-07
	$\varepsilon''_{e_{1g}(\epsilon)}$	-3.56E-07	-1.24E-07	2.94E-07	4.46E-07	-6.09E-08
	$\varepsilon''_{e_{2u}(\theta)}$	-2.03E-07	2.35E-07	3.67E-07	2.82E-07	-2.44E-08
	$\varepsilon''_{e_{2u}(\epsilon)}$	-2.03E-06	-1.69E-06	-1.39E-06	-1.51E-06	-1.91E-06
$\nu_{2e_{2g}(\theta)}$	$\varepsilon''_{e_{1g}(\theta)}$	-1.37E-06	-1.75E-06	-1.39E-06	-7.82E-07	-1.60E-06
	$\varepsilon''_{e_{1g}(\epsilon)}$	-1.53E-06	-2.01E-06	-1.68E-06	-1.27E-06	-1.85E-06
	$\varepsilon''_{e_{2u}(\theta)}$	-5.59E-07	-5.33E-07	-3.86E-07	-4.65E-07	-6.46E-07
	$\varepsilon''_{e_{2u}(\epsilon)}$	-1.93E-06	-1.79E-06	-1.67E-06	-1.57E-06	-1.87E-06
$\nu_{3e_{2g}(\theta)}$	$\varepsilon''_{e_{1g}(\theta)}$	-4.80E-07	-9.22E-07	-1.26E-07	-1.93E-07	-7.20E-07
	$\varepsilon''_{e_{1g}(\epsilon)}$	-3.16E-06	-3.36E-06	-3.04E-06	-2.96E-06	-3.31E-06
	$\varepsilon''_{e_{2u}(\theta)}$	1.84E-06	2.17E-06	2.22E-06	1.92E-06	1.95E-06
	$\varepsilon''_{e_{2u}(\epsilon)}$	-1.86E-06	-1.53E-06	-1.20E-06	-1.42E-06	-1.64E-06
$\nu_{4e_{2g}(\theta)}$	$\varepsilon''_{e_{1g}(\theta)}$	-4.08E-06	-3.95E-06	-3.19E-06	-3.80E-06	-3.61E-06
	$\varepsilon''_{e_{1g}(\epsilon)}$	-4.00E-06	-4.38E-06	-3.52E-06	-3.71E-06	-3.87E-06
	$\varepsilon''_{e_{2u}(\theta)}$	-3.97E-06	-3.90E-06	-3.32E-06	-3.71E-06	-3.55E-06
	$\varepsilon''_{e_{2u}(\epsilon)}$	-4.73E-06	-4.57E-06	-4.00E-06	-4.33E-06	-4.23E-06

Lastly, the two minimal energy points on the PES for the benzene cation and anion can be obtained using Equation (11), and are given as:

$$E_{\pm}^{(2)} = \frac{(V_{e_{2g}(\theta)}^{(1)})^2}{2(V_{a'_{1g}}^{(2)} \pm V_{e_{2g}(\theta)}^{(2)})} \tag{19}$$

where the factor of $1/\sqrt{2}$ is absorbed into the second order V_i terms in the fitting process. The JT stabilisation energies is given in Table S17, and it can be seen that the energy difference between the two minimum points is small.

TABLE S16. Effect of extending the linear vibronic coupling model to include second order terms on the calculated vibrational frequencies of the benzene cation and anion.. All values are in cm^{-1} .

		evGW@				
Mode		BLYP	B3LYP	CAM-B3LYP	tCAM-B3LYP	IP-tCAM-B3LYP
ω_{1a_1g}	Neutral	1010	1015	1021	1014	1019
	$ E_{1g}(\theta)\rangle$	1014	1029	1031	1025	1027
	$ E_{1g}(\epsilon)\rangle$	1013	1028	1031	1026	1026
	$ E_{2u}(\theta)\rangle$	987	1009	1005	999	1002
	$ E_{2u}(\epsilon)\rangle$	989	1009	1003	998	1004
ω_{2a_1g}	Neutral	3208	3195	3246	3229	3250
	$ E_{1g}(\theta)\rangle$	3223	3217	3261	3247	3267
	$ E_{1g}(\epsilon)\rangle$	3223	3213	3261	3247	3267
	$ E_{2u}(\theta)\rangle$	3222	3212	3260	3245	3252
	$ E_{2u}(\epsilon)\rangle$	3221	3211	3260	3245	3253
$\omega_{1e_2g(\theta)}$	Neutral	614	624	633	617	624
	$ E_{1g}(\theta)\rangle$	628	629	621	600	626
	$ E_{1g}(\epsilon)\rangle$	609	602	600	582	607
	$ E_{2u}(\theta)\rangle$	622	615	618	606	625
	$ E_{2u}(\epsilon)\rangle$	689	686	683	674	694
$\omega_{2e_2g(\theta)}$	Neutral	1178	1200	1209	1180	1187
	$ E_{1g}(\theta)\rangle$	1209	1240	1242	1206	1224
	$ E_{1g}(\epsilon)\rangle$	1205	1235	1237	1196	1219
	$ E_{2u}(\theta)\rangle$	1216	1235	1242	1212	1224
	$ E_{2u}(\epsilon)\rangle$	1189	1211	1217	1189	1200
$\omega_{3e_2g(\theta)}$	Neutral	1614	1637	1659	1631	1651
	$ E_{1g}(\theta)\rangle$	1661	1686	1703	1674	1698
	$ E_{1g}(\epsilon)\rangle$	1621	1651	1661	1634	1661
	$ E_{2u}(\theta)\rangle$	1642	1659	1677	1652	1675
	$ E_{2u}(\epsilon)\rangle$	1587	1605	1627	1602	1622
$\omega_{4e_2g(\theta)}$	Neutral	3204	3170	3242	3227	3247
	$ E_{1g}(\theta)\rangle$	3235	3200	3266	3255	3274
	$ E_{1g}(\epsilon)\rangle$	3234	3203	3268	3254	3275
	$ E_{2u}(\theta)\rangle$	3240	3205	3272	3259	3278
	$ E_{2u}(\epsilon)\rangle$	3234	3200	3267	3254	3273

TABLE S17. Effect of extending the linear vibronic coupling model to include second order terms on the JT stabilisation energies of the benzene cation and anion (QJT). The DFT frequencies of neutral benzene were used in the calculation. All values are in cm^{-1} .

		evGW@				
Mode		BLYP	B3LYP	CAM-B3LYP	tCAM-B3LYP	IP-tCAM-B3LYP
$E_{1a_1g}^{JT}$	Linear JT	251	230	224	235	228
	$ E_{1g}(\theta)\rangle$ (QJT)	249	224	220	231	225
	$ E_{1g}(\epsilon)\rangle$ (QJT)	250	224	220	230	225
	Linear JT	584	605	604	596	600
	$ E_{2u}(\theta)\rangle$ (QJT)	609	612	626	616	619
	$ E_{2u}(\epsilon)\rangle$ (QJT)	612	613	624	615	621
$E_{2a_1g}^{JT}$	Linear JT	7	7	5	5	4
	$ E_{1g}(\theta)\rangle$ (QJT)	7	7	5	5	4
	$ E_{1g}(\epsilon)\rangle$ (QJT)	7	7	5	5	4
	Linear JT	1	1	0	0	1
	$ E_{2u}(\theta)\rangle$ (QJT)	1	1	0	0	1
	$ E_{2u}(\epsilon)\rangle$ (QJT)	1	1	0	0	1
$E_{1e_2g(\theta)}^{JT}$	Linear JT	322	316	317	323	324
	$ E_{1g}(\theta)\rangle$ (QJT)	327	340	346	365	342
	$ E_{1g}(\epsilon)\rangle$ (QJT)	308	311	323	343	322
	Linear JT	46	44	43	45	44
	$ E_{2u}(\theta)\rangle$ (QJT)	44	46	47	47	44
	$ E_{2u}(\epsilon)\rangle$ (QJT)	36	37	38	38	35
$E_{2e_2g(\theta)}^{JT}$	Linear JT	192	180	174	189	186
	$ E_{1g}(\theta)\rangle$ (QJT)	182	171	168	182	173
	$ E_{1g}(\epsilon)\rangle$ (QJT)	181	170	167	179	171
	Linear JT	254	250	245	255	249
	$ E_{2u}(\theta)\rangle$ (QJT)	242	231	229	241	240
	$ E_{2u}(\epsilon)\rangle$ (QJT)	253	241	239	250	250
$E_{3e_2g(\theta)}^{JT}$	Linear JT	582	558	543	565	545
	$ E_{1g}(\theta)\rangle$ (QJT)	578	553	540	560	535
	$ E_{1g}(\epsilon)\rangle$ (QJT)	551	530	513	533	512
	Linear JT	725	707	676	699	676
	$ E_{2u}(\theta)\rangle$ (QJT)	695	677	660	680	656
	$ E_{2u}(\epsilon)\rangle$ (QJT)	744	723	701	723	699
$E_{4e_2g(\theta)}^{JT}$	Linear JT	0	0	0	0	0
	$ E_{1g}(\theta)\rangle$ (QJT)	0	0	0	0	0
	$ E_{1g}(\epsilon)\rangle$ (QJT)	0	0	0	0	0
	Linear JT	9	8	8	8	8
	$ E_{2u}(\theta)\rangle$ (QJT)	8	8	8	8	8
	$ E_{2u}(\epsilon)\rangle$ (QJT)	8	8	8	8	8

S7. PLOT OF ORBITAL AND QUASIPARTICLE ENERGIES

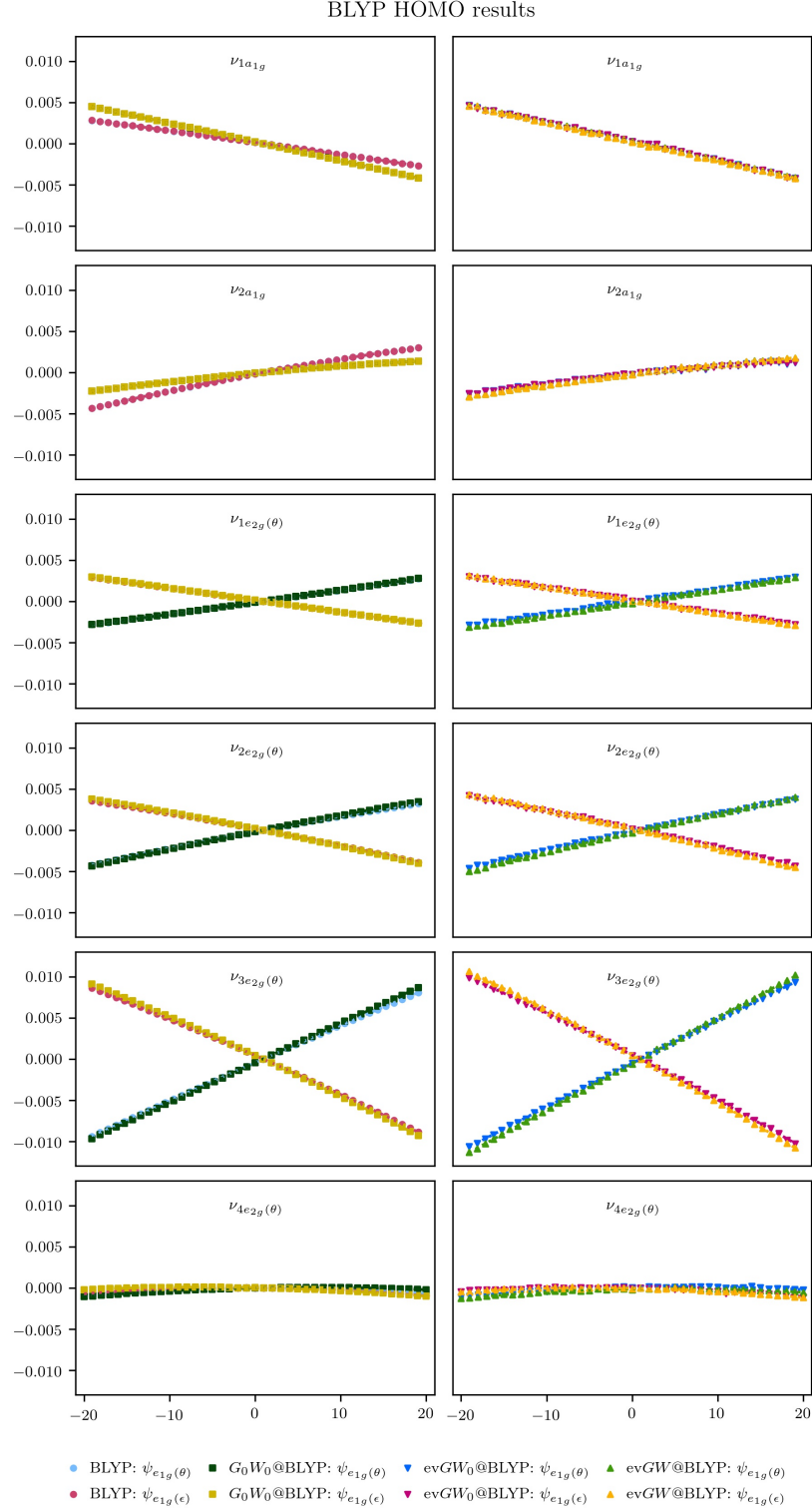


FIG. S2. DFT (BLYP) Kohn-Sham orbital and *GW* quasiparticle energies for the degenerate HOMOs of neutral benzene with respect to a distortion along the a_{1g} and e_{2g} normal modes. The energies were vertically shifted to set the energies at R_0 to be zero.

B3LYP HOMO results

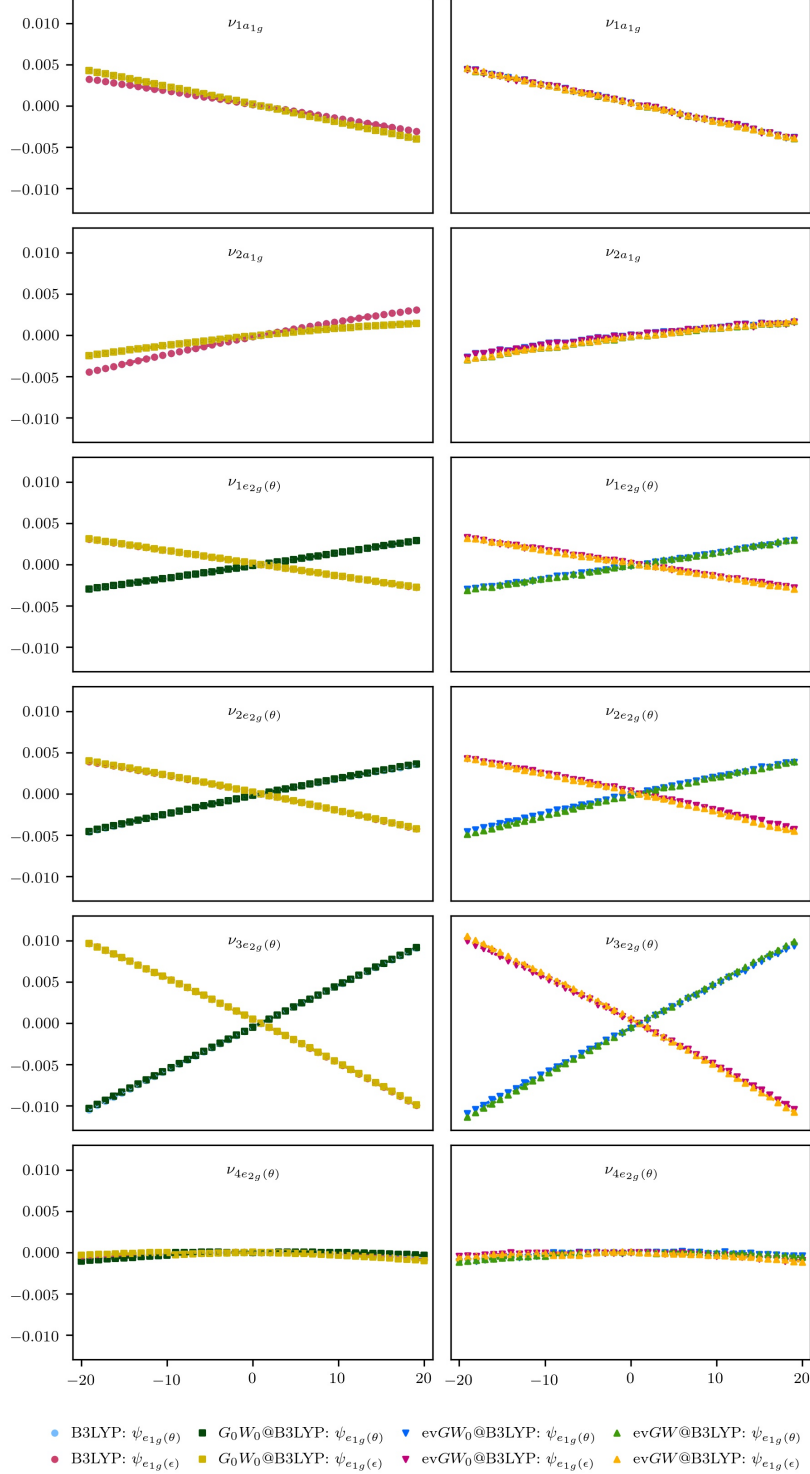


FIG. S3. DFT (B3LYP) Kohn-Sham orbital and *GW* quasiparticle energies for the degenerate HOMOs of neutral benzene with respect to a distortion along the a_{1g} and e_{2g} normal modes. The energies were vertically shifted to set the energies at R_0 to be zero.

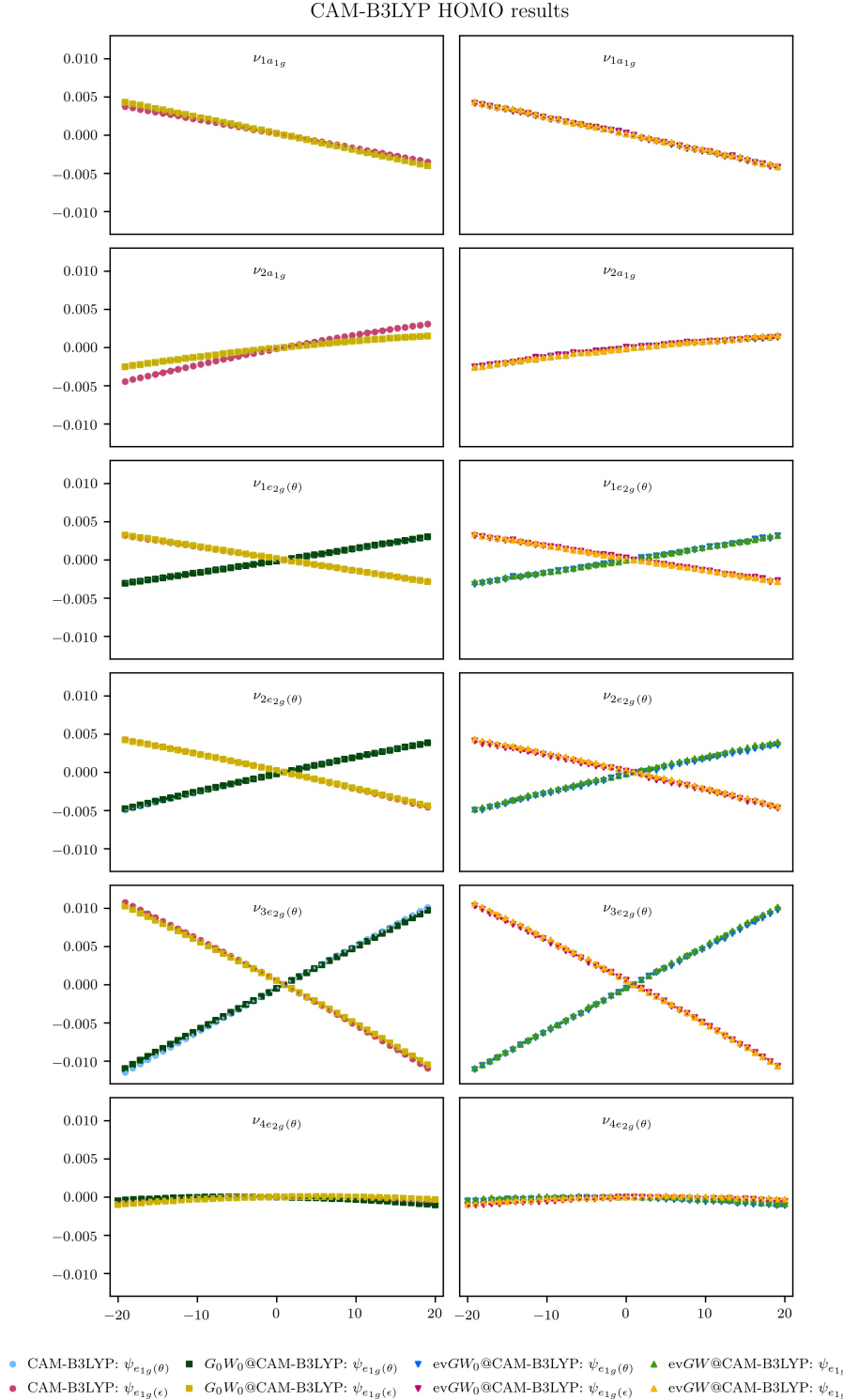


FIG. S4. DFT (CAM-B3LYP) Kohn-Sham orbital and *GW* quasiparticle energies for the degenerate HOMOs of neutral benzene with respect to a distortion along the a_{1g} and e_{2g} normal modes. The energies were vertically shifted to set the energies at R_0 to be zero.

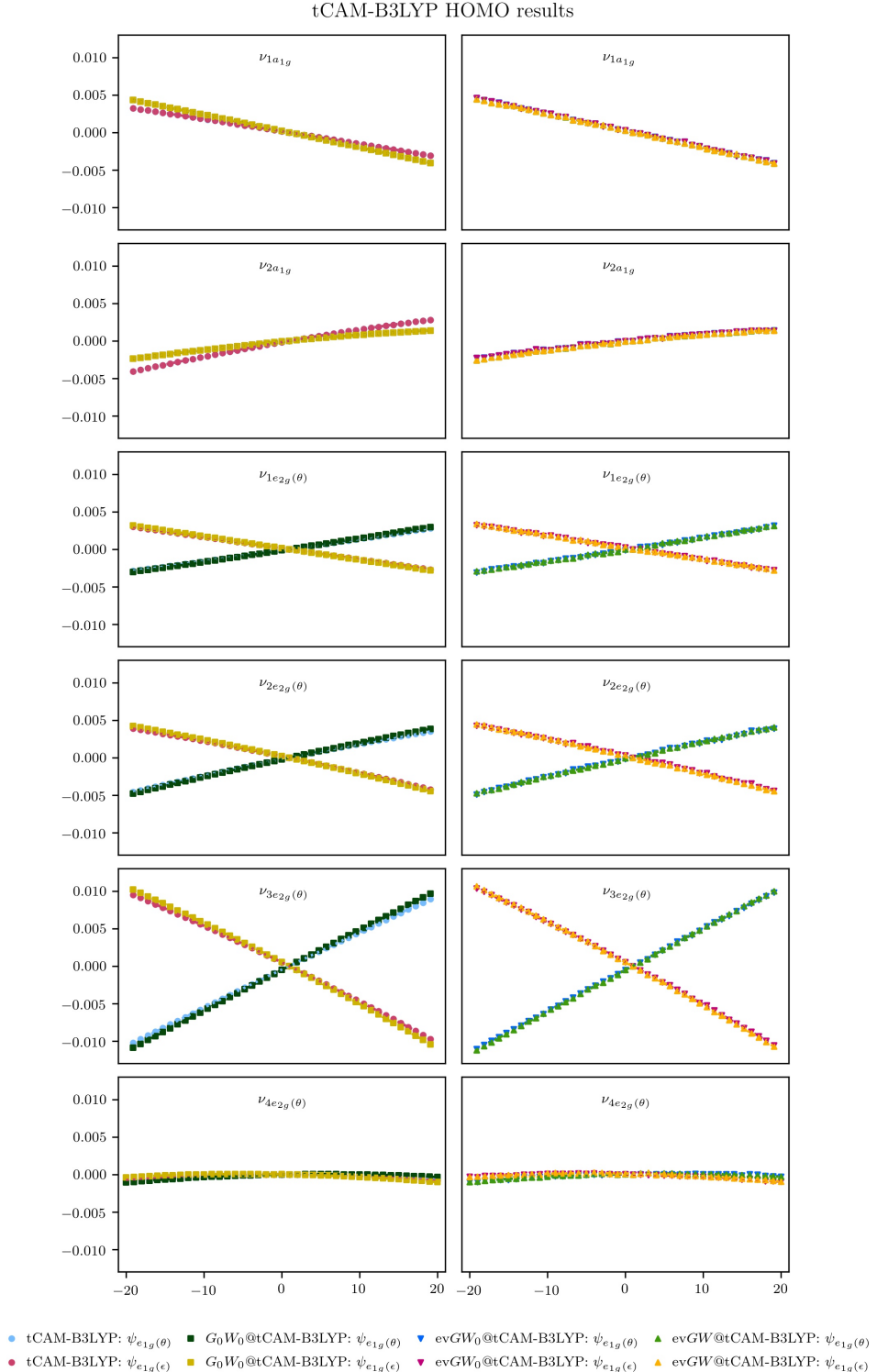


FIG. S5. DFT (CAM-B3LYP) Kohn-Sham orbital and *GW* quasiparticle energies for the degenerate HOMOs of neutral benzene with respect to a distortion along the a_{1g} and e_{2g} normal modes. The energies were vertically shifted to set the energies at R_0 to be zero.

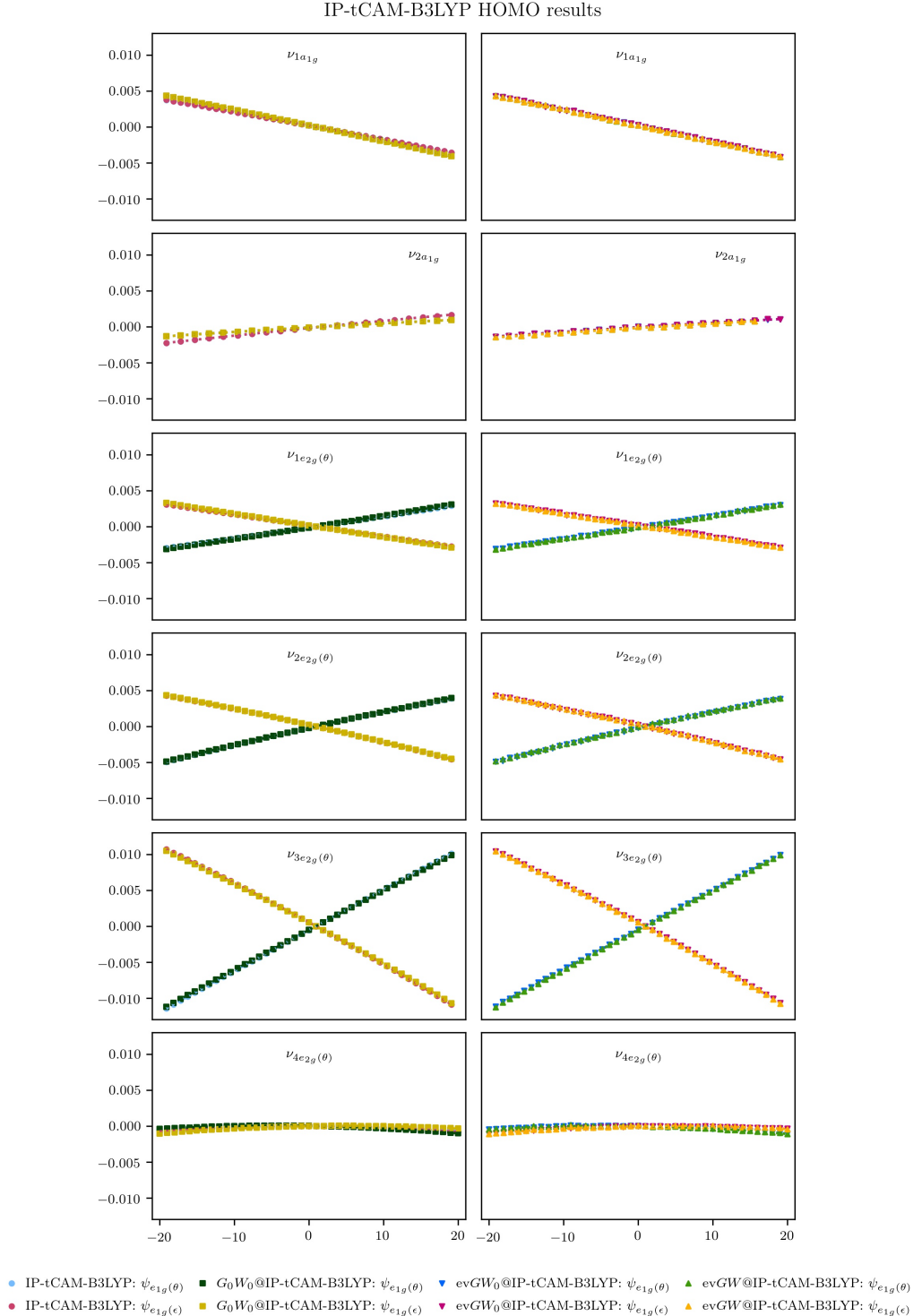


FIG. S6. DFT (CAM-B3LYP) Kohn-Sham orbital and *GW* quasiparticle energies for the degenerate HOMOs of neutral benzene with respect to a distortion along the a_{1g} and e_{2g} normal modes. The energies were vertically shifted to set the energies at R_0 to be zero.

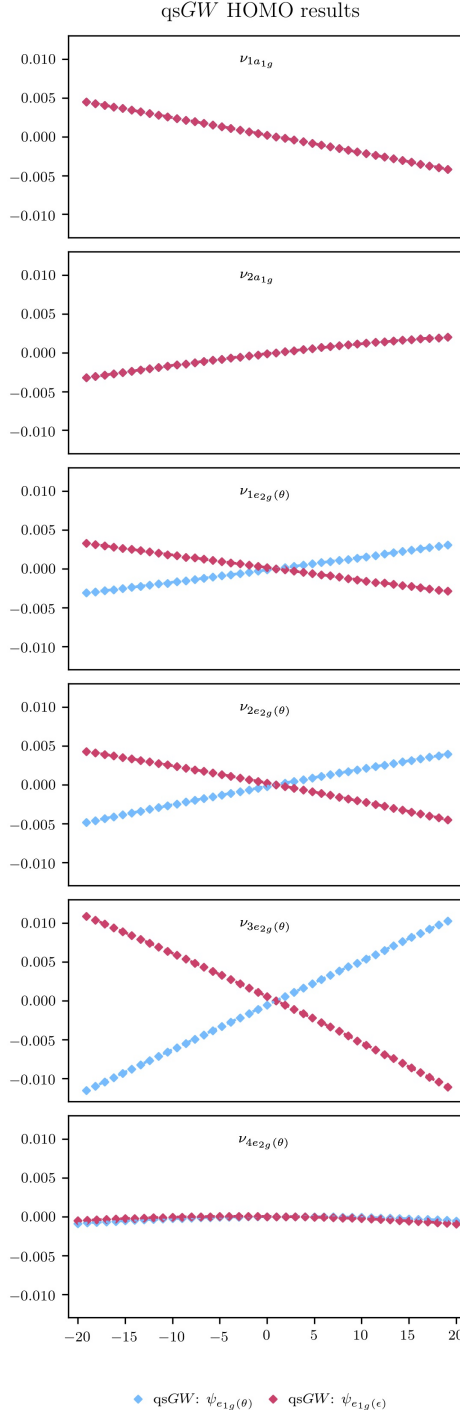


FIG. S7. qsGW quasiparticle energies for the degenerate HOMOs of neutral benzene with respect to a distortion along the a_{1g} and e_{2g} normal modes. The energies were vertically shifted to set the energies at R_0 to be zero.

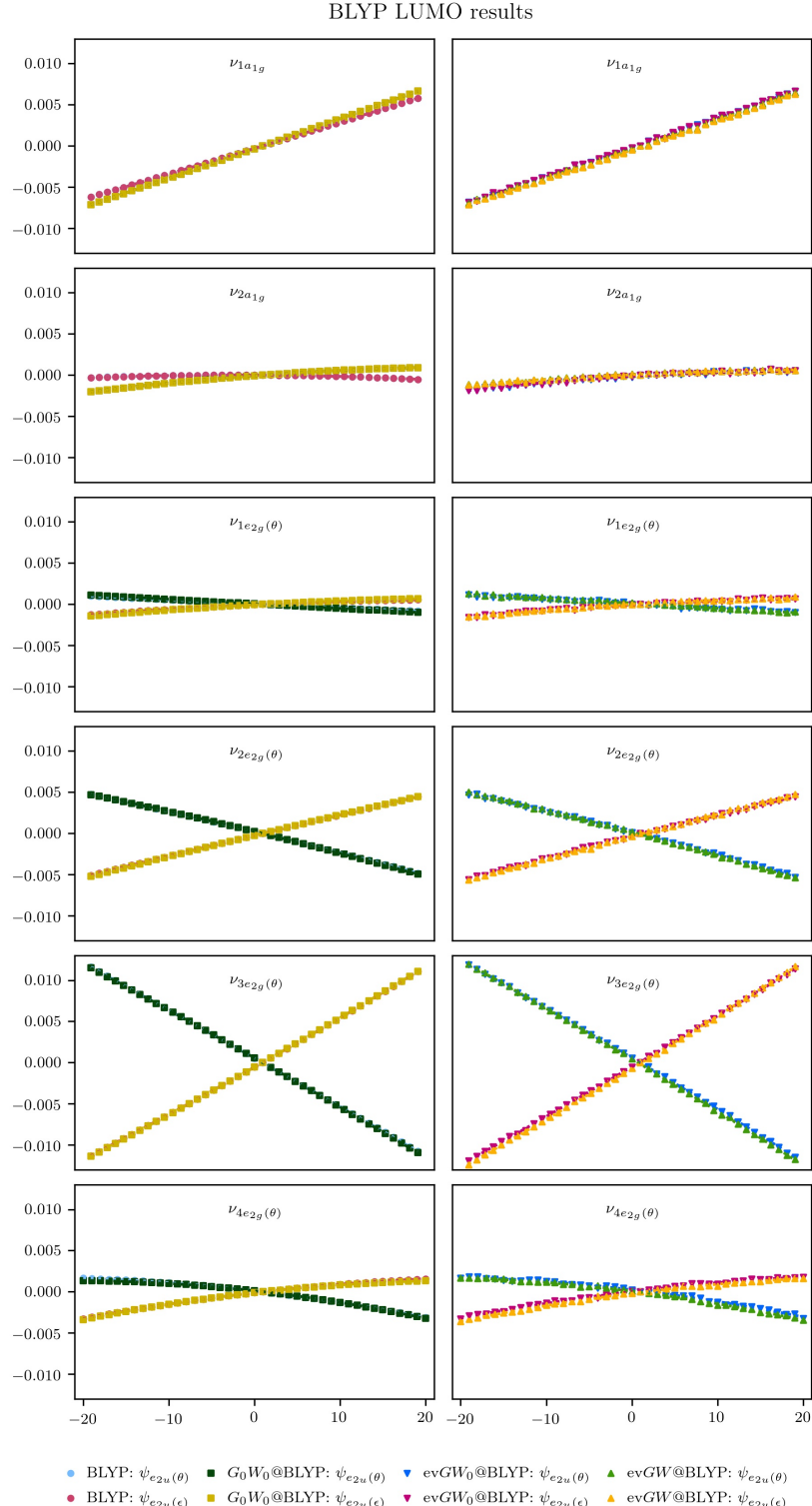


FIG. S8. DFT (BLYP) Kohn-Sham orbital and *GW* quasiparticle energies for the degenerate LUMOs of neutral benzene with respect to a distortion along the a_{1g} and e_{2g} normal modes. The energies were vertically shifted to set the energies at R_0 to be zero.

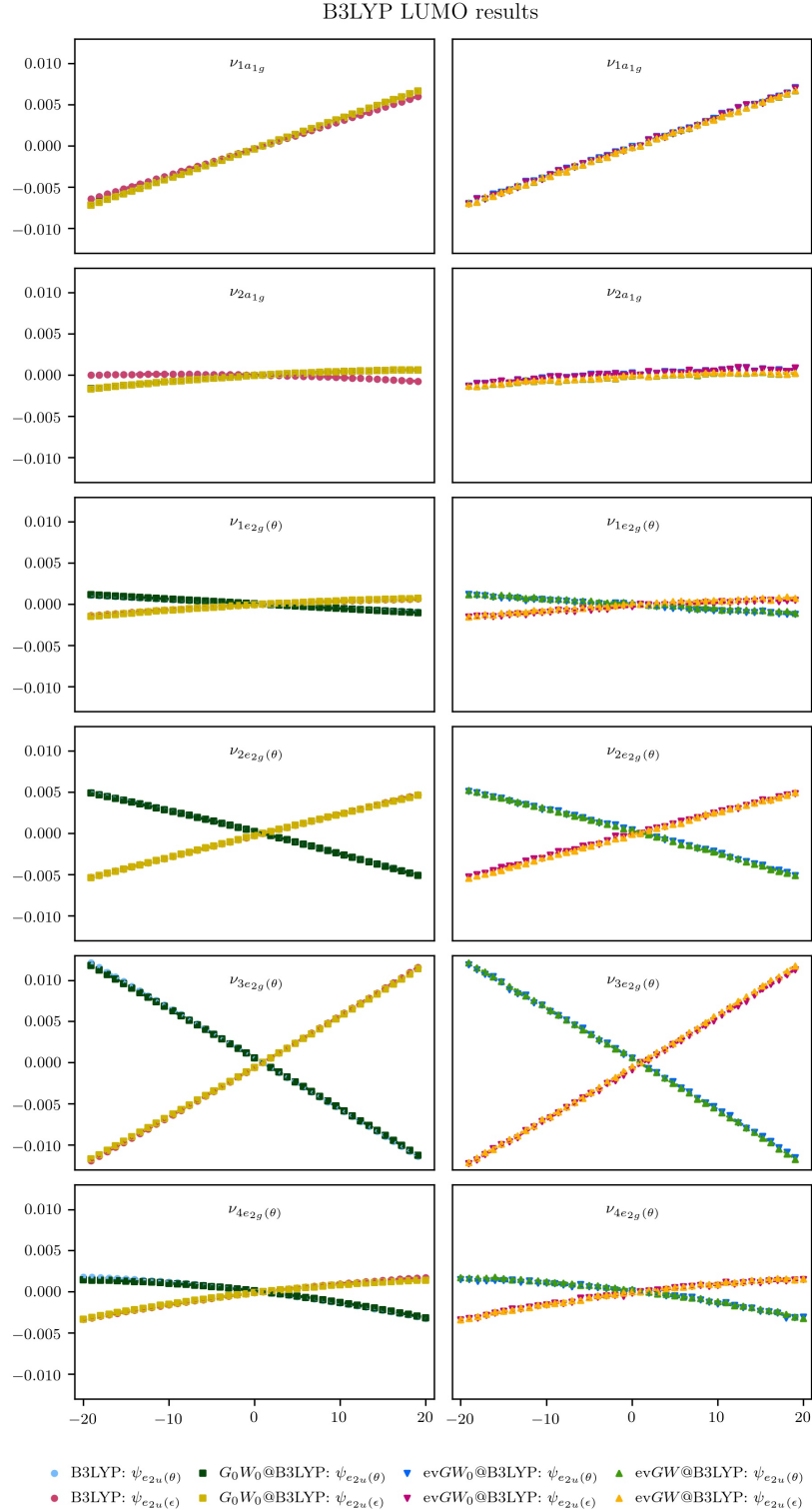


FIG. S9. DFT (B3LYP) Kohn-Sham orbital and *GW* quasiparticle energies for the degenerate LUMOs of neutral benzene with respect to a distortion along the a_{1g} and e_{2g} normal modes. The energies were vertically shifted to set the energies at R_0 to be zero.

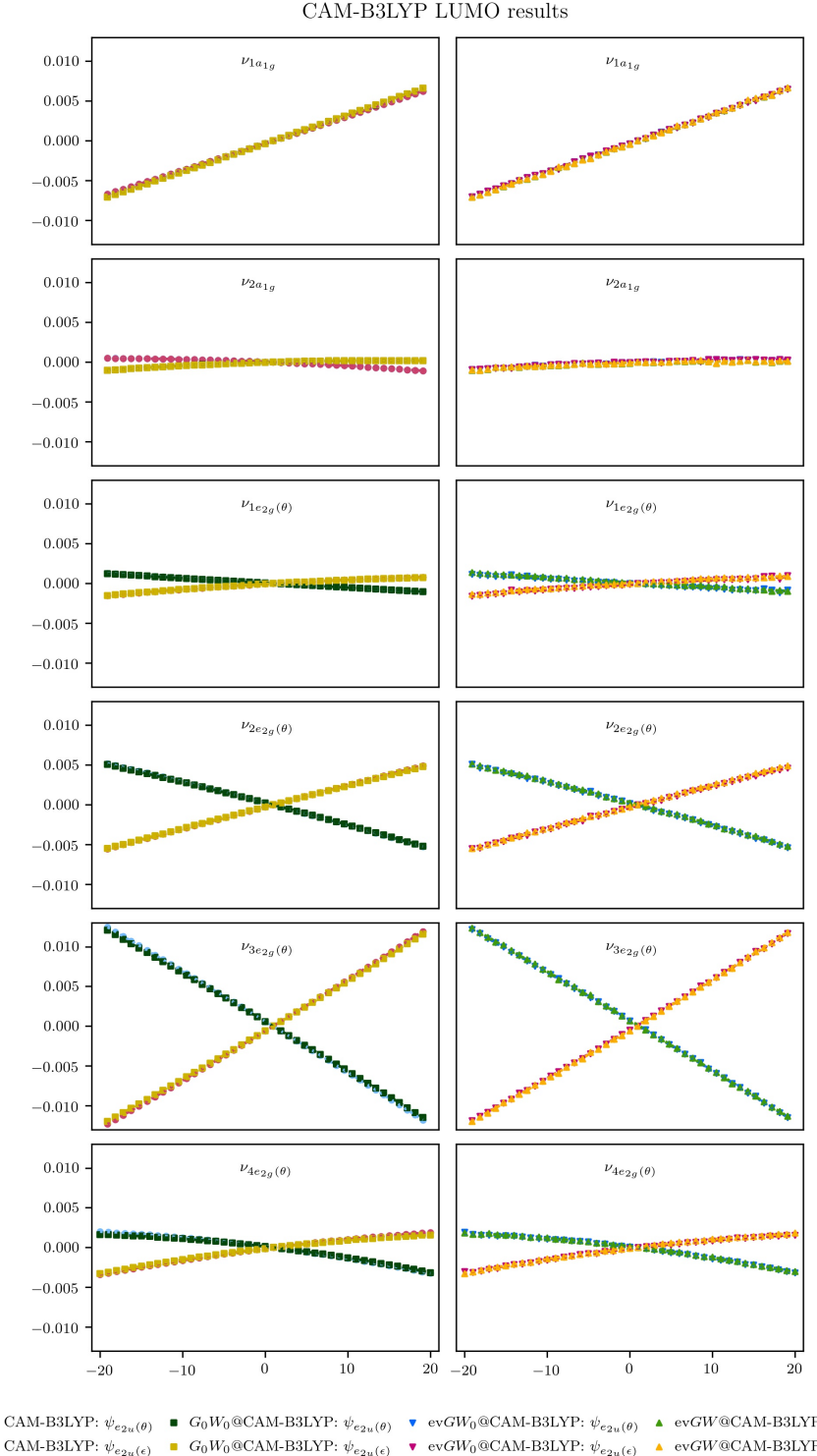


FIG. S10. DFT (CAM-B3LYP) Kohn-Sham orbital and GW quasiparticle energies for the degenerate LUMOs of neutral benzene with respect to a distortion along the a_{1g} and e_{2g} normal modes. The energies were vertically shifted to set the energies at R_0 to be zero.

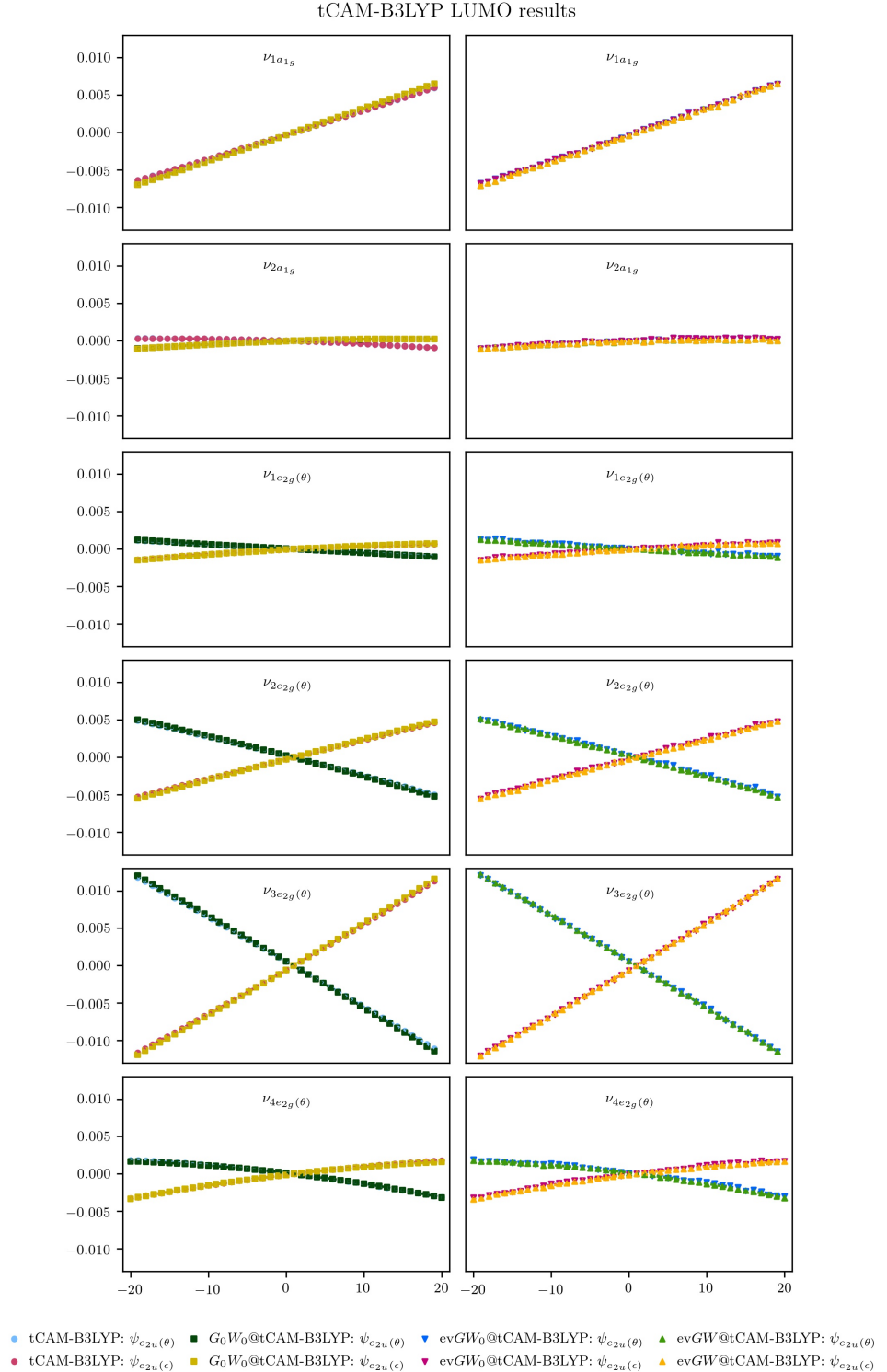


FIG. S11. DFT (CAM-B3LYP) Kohn-Sham orbital and GW quasiparticle energies for the degenerate LUMOs of neutral benzene with respect to a distortion along the a_{1g} and e_{2g} normal modes. The energies were vertically shifted to set the energies at R_0 to be zero.

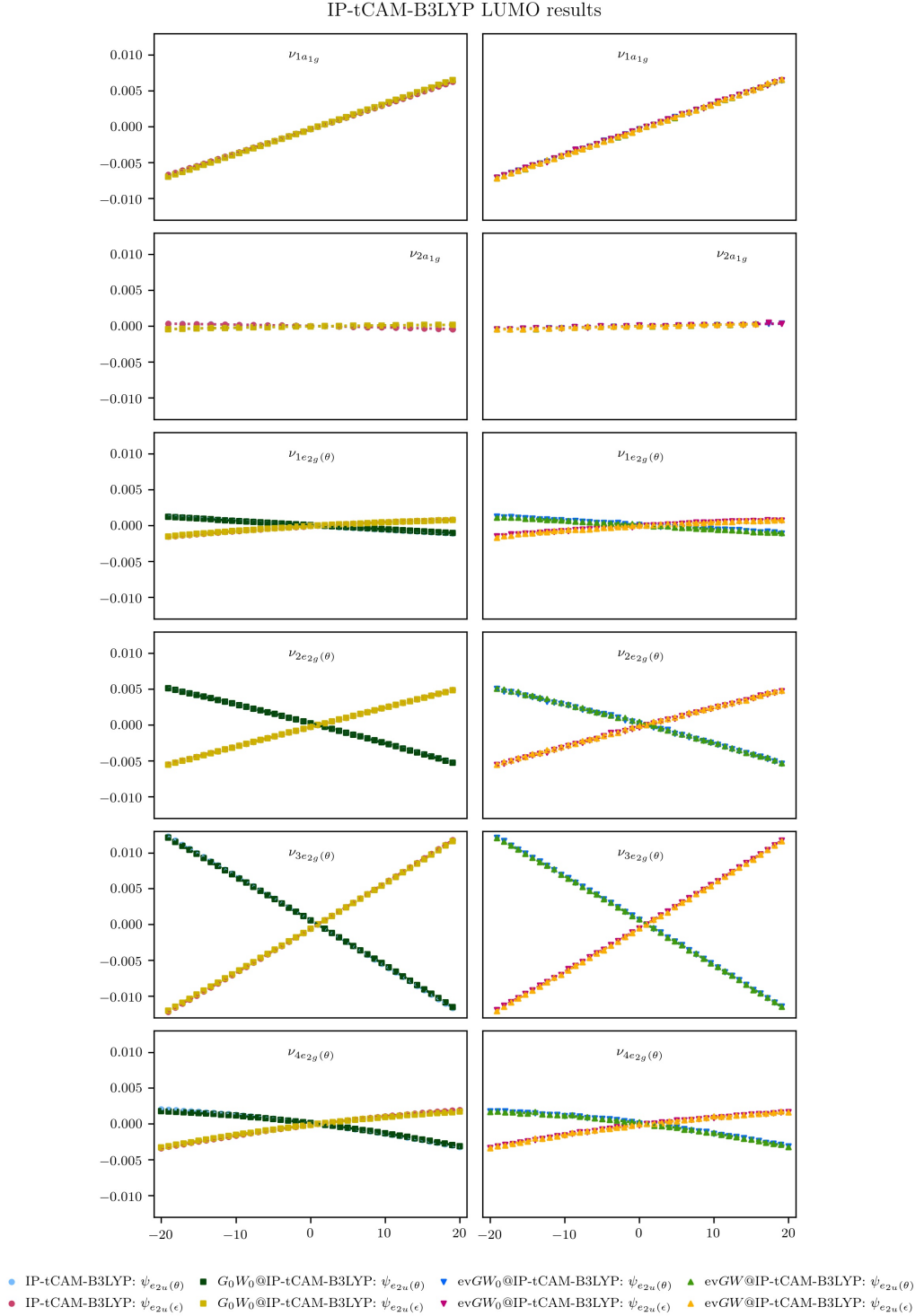


FIG. S12. DFT (CAM-B3LYP) Kohn-Sham orbital and *GW* quasiparticle energies for the degenerate LUMOs of neutral benzene with respect to a distortion along the a_{1g} and e_{2g} normal modes. The energies were vertically shifted to set the energies at R_0 to be zero.

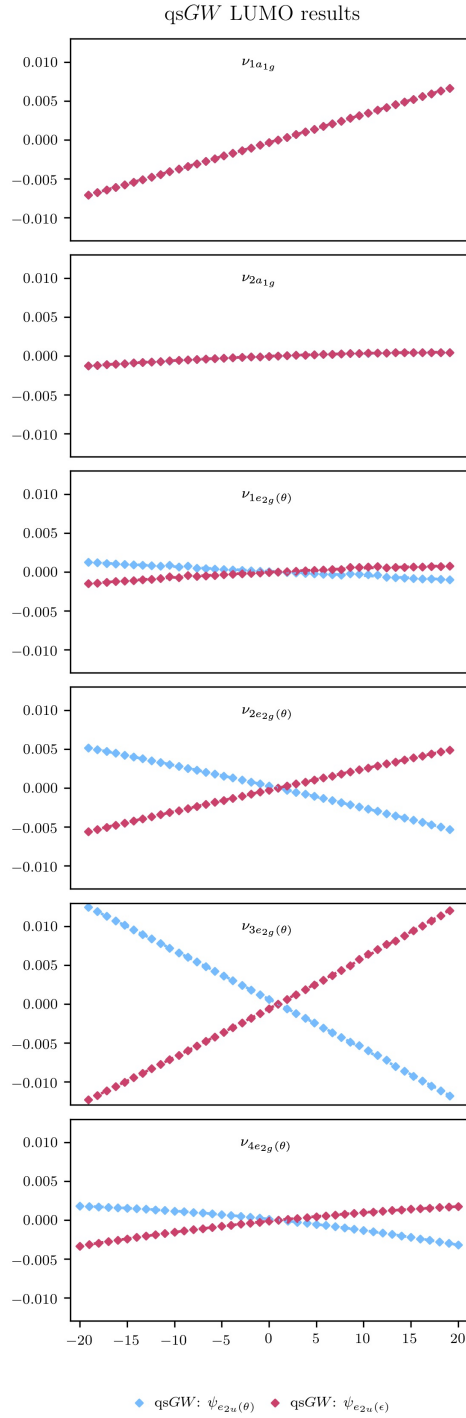


FIG. S13. qsGW quasiparticle energies for the degenerate LUMOs of neutral benzene with respect to a distortion along the a_{1g} and e_{2g} normal modes. The energies were vertically shifted to set the energies at R_0 to be zero.

REFERENCES

- ¹M. Srebro and J. Autschbach, “Does a molecule-specific density functional give an accurate electron density? the challenging case of the CuCl electric field gradient,” *The Journal of Physical Chemistry Letters* **3**, 576–581 (2012).
- ²J. Autschbach and M. Srebro, “Delocalization error and “functional tuning” in kohn–sham calculations of molecular properties,” *Accounts of Chemical Research* **47**, 2592–2602 (2014).
- ³T. Yanai, D. P. Tew, and N. C. Handy, “A new hybrid exchange–correlation functional using the coulomb-attenuating method (cam-b3lyp),” *Chemical Physics Letters* **393**, 51–57 (2004).
- ⁴K. Okuno, Y. Shigeta, R. Kishi, H. Miyasaka, and M. Nakano, “Tuned cam-b3lyp functional in the time-dependent density functional theory scheme for excitation energies and properties of diarylethene derivatives,” *Journal of Photochemistry and Photobiology A: Chemistry* **235**, 29–34 (2012).
- ⁵S. Lehtola, C. Steigemann, M. J. T. Oliveira, and M. A. L. Marques, “Recent developments in libxc — a comprehensive library of functionals for density functional theory,” *SoftwareX* **7**, 1–5 (2018).
- ⁶T. Rangel, S. M. Hamed, F. Bruneval, and J. B. Neaton, “Evaluating the GW approximation with CCSD(t) for charged excitations across the oligoacenes,” *Journal of Chemical Theory and Computation* **12**, 2834–2842 (2016).
- ⁷R. D. Johnson, “Nist computational chemistry comparison and benchmark database,” (1999).